Mon. Not. R. Astron. Soc. **337,** 749–767 (2002)

The Galactic distribution of asymptotic giant branch stars

Tom Jackson,★ Željko Ivezić★ and G. R. Knapp★
Princeton University, Department of Astrophysical Sciences, Princeton, NJ 08544-1001, USA

Accepted 2002 August 10. Received 2002 August 6; in original form 2002 February 22

ABSTRACT

We study the Galactic distribution of ∼10 000 candidate asymptotic giant branch (AGB) stars selected by *IRAS* colours and variability index. The distance to each star is estimated by assuming a narrow luminosity function and a model-derived bolometric correction. The characteristic AGB star luminosity, $L_{\rm AGB}$, is determined from the condition that the highest number density must coincide with the Galactic bulge. Assuming a bulge distance of 8 kpc, we determine $L_{\rm AGB} \sim 3500$ L$_\odot$, in close agreement with values obtained for nearby AGB stars using the *Hipparcos* data, and those obtained by other methods.

We find that there are no statistically significant differences in the Galactic distribution of AGB stars with different *IRAS* colours, implying a universal density distribution. The direct determination of this distribution shows that it is separable in the radial, R, and vertical, z, directions. Perpendicular to the Galactic plane, the number density of AGB stars is well described by an exponential function with a vertical scaleheight of 300 pc. In the radial direction the number density of AGB stars is constant up to $R \sim 5$ kpc, and then it decreases exponentially with a scalelength of ∼1.6 kpc. This fall-off extends to at least 12 kpc, where the sample becomes too small. The overall normalization implies that there are ∼200 000 AGB stars in the Galaxy.

We estimate the [25]–[12] colour distribution of AGB stars for an unbiased volume-limited sample. By using a model-dependent transformation between the colour and mass-loss rate, $\dot{M}$, we constrain the time dependence of $\dot{M}$. The results suggest that for $10^{-6} < \dot{M} < 10^{-5}$ M$_\odot$ yr^{-1} the mass-loss rate increases exponentially with time. We find only marginal evidence that the mass-loss rate increases with stellar mass.

Key words: stars: AGB and post-AGB – stars: evolution – stars: mass-loss.

1 INTRODUCTION

Studies of the stellar distribution within the Galaxy can provide information on its formation mechanism(s) and subsequent evolution. While a significant amount of data concerning the Galaxy has been collected over the years, knowledge of the stellar distribution in the Galactic plane is still limited to a few kpc from the Sun (Mihalas & Binney 1981; Binney & Tremaine 1987) by interstellar dust extinction because the visual extinction is already 1 mag at a distance of only ∼0.6 kpc (Spitzer 1978).

The interstellar dust extinction decreases with wavelength and is all but negligible beyond approximately 10 μm, even for stars at the Galactic Centre. For this reason, the analysis of the data obtained by the *Infrared Astronomical Satellite* (*IRAS*, Beichman et al. 1985) has significantly enhanced our knowledge of the stellar distribution in the Galactic disc and bulge. *IRAS* surveyed 96 per cent of the sky at 12, 25, 60 and 100 μm, with the resulting point source catalogue (*IRAS* PSC) containing over 250 000 sources. The colours based on *IRAS* fluxes[1] can efficiently be used to distinguish pre-main-sequence from post-main-sequence stars, and to study characteristics of their dust emission (e.g. van der Veen & Habing 1988; Ivezić & Elitzur 2000, hereafter IE00).

Soon after the *IRAS* data became available it was realized that properly colour-selected point sources clearly outline the disc and the bulge (Habing et al. 1985). The colour selection corresponds to OH/infrared (IR) stars, asymptotic giant branch (AGB) stars with very thick dust shells caused by intensive mass loss (for a detailed review see Habing 1996). Because these stars have large luminosity (∼10^3–10^4 L$_\odot$), and because a large fraction of that luminosity is radiated in the mid-IR caused by reprocessing by circumstellar dust, they are brighter than the *IRAS* faint cut-off (<1 Jy at 12 μm) even at the distance of the Galactic Centre. The availability of *IRAS* data soon prompted several detailed studies of the Galactic distribution of AGB stars. Common features in all of these studies are the sample

★E-mail: jackson@astro.Princeton.edu (TJ); ivezic@astro.Princeton.edu (ZI); gk@astro.Princeton.edu (GRK).

[1] Except when discussing bolometric flux, the implied meaning of 'flux' is the flux density.

selection based on the *IRAS* F_{12} versus [25]–[12] colour–magnitude diagram, and the determination of the bolometric flux by utilizing a model-based bolometric correction.

Habing et al. (1985) discuss ∼7000 bulge stars selected by $0.5 < F_{12}/F_{25} < 1.5$ and $1 < F_{12} < 5$ Jy, in two areas defined by $|b| < 10^\circ$, $|l| < 10^\circ$ and $|b| < 10^\circ$, $10^\circ < l < 30^\circ$. Assuming that for all stars $F_{12} = 2.3$ Jy, and a bolometric correction calculated for a $T = 350$-K blackbody, they derive $L_{\rm bol} = 2600\,{\rm L}_\odot$ [for the Galactic Centre distance of 8 kpc Reid (1989)]. They also find that 25 per cent of the selected sources have an *IRAS* variability index (the probability that a source is variable, expressed in per cent, for a definition see Section 2.2) larger than 99, as compared with 13 per cent for all stars from the *IRAS* PSC. This difference is in good agreement with the known long-period variability of AGB stars. Habing et al. (1985) also noted that despite this agreement, their sample may still be severely contaminated by planetary nebulae. They classified 2 per cent of stars from the sample using supplemental data and found the same fractions of variable stars and planetary nebulae.

Rowan-Robinson & Chester (1987) select bulge stars by requiring $F_{12} > 1$ Jy (interpreted as the *IRAS* confusion limit) and $|b| < 10^\circ$, $|l| < 10^\circ$. They assumed that all of these objects in the *direction* of the Galactic Centre are actually *at* the Galactic Centre. This assumption allowed them to determine the median luminosity (∼3000 $\rm L_\odot$) and to place an upper limit on the width of the luminosity function, which was found to be very narrow (the root-mean-square scatter is approximately a factor of 2). They also determined the distribution of colours and transformed it into a distribution of the shell optical depth by using model-dependent transformations. Assuming that this luminosity function and optical depth distribution also apply to the Galactic disc, and that the disc volume density distribution can be parametrized as two separable exponential functions in the vertical, z, and radial, R, directions, they derive a scaleheight of 250 pc and a scalelength of 6 kpc.

Habing (1988) extended the analysis to disc sources in several areas on the sky defined as thin strips parallel to the Galactic equator, with a total area of 1200 $\rm deg^2$, or approximately 3 per cent of the sky. AGB stars are selected by requiring $F_{12} > 1$ Jy, $0.3 < F_{25}/F_{12} < 3.8$ and $q_{12} = q_{25} = 3$, where q_{12} and q_{25} are *IRAS* flux qualities at 12 and 25 μm (1, upper limit; 2, low quality; 3, high quality). Habing does not include the 60-μm flux in the source selection because the resulting number of sources is too small, but does exclude those sources for which $F_{60} > F_{25}$ is reliably measured. This sample was used to constrain the luminosity function and spatial distribution of stars by fitting number counts in the selected areas. The spatial distribution is assumed to be separable: a $\rm sech^2$ function for the z-direction with an R-independent scaleheight (this was motivated by results obtained for other galaxies), and an exponential for the R-direction. Habing finds that the models are not unique, and it is hard to find a best-fitting one. He concludes that the sample contained two populations with either a similar spatial density and different luminosities, or a similar luminosity but different spatial distributions. Habing prefers the second option and argues that the results present evidence for the thick disc proposed by Gilmore & Reid (1983), and for a thin disc cut-off at $R \sim 10$ kpc. He also points out that the luminosity function in the disc is similar to that in the bulge, providing support for the earlier assumption by Rowan-Robinson & Chester (1987).

Blommaert, van der Veen & Habing (1993) extended the study by Habing (1988) with the aim of determining the sample contamination. They obtained near-IR photometry and OH maser measurements for 53 sources, which are located outside the solar circle and have $F_{25} > F_{12}$ (region IIIb of the *IRAS* colour–colour diagram, as defined by van der Veen & Habing 1988). Although this subsample is expected to have the least amount of contamination by non-AGB stars, they find that ∼55 per cent of objects are not AGB stars. The contaminating sources have overestimated distances caused by both underestimated bolometric corrections and overestimated luminosities, and resulted in spurious evidence for a thick disc and the thin disc cut-off.

These pioneering *IRAS*-based studies suggested that the luminosity function for AGB stars is rather narrow and centred around $L \sim 3000\,{\rm L}_\odot$, and appears not to vary strongly with position in the Galaxy. The *IRAS* number counts can be reasonably well fitted by assuming a spatial distribution of AGB stars that is separable in z and R, and described by exponential functions with a scaleheight of 250 pc and a scalelength of 6 kpc, respectively.

In this work we revisit the problem of constraining the Galactic distribution of AGB stars using *IRAS* data. There are several factors motivating us to perform a study similar to those listed above.

(i) The study by Blommaert et al. (1993) showed that the variability index is a reliable indicator of AGB stars, while samples selected by colours alone can be significantly contaminated. Thus, it seems prudent to complement the sample colour selection by using the *IRAS* variability index and repeating the analysis. Furthermore, the understanding of the *IRAS* colour–colour diagrams and the distribution of various types of dusty star has advanced since the early studies of *IRAS* data, and can be used to select cleaner, more reliable samples (e.g. van der Veen & Habing 1988; IE00).

(ii) The spectral energy distribution (SED) models for AGB stars and their dependence on the various stellar parameters are also better understood. In particular, more reliable bolometric corrections are available, and the *IRAS* colours are recognized as an indicator of the mass-loss rate (Habing 1996 and references therein).

(iii) The *Hipparcos* data allowed direct determination of the bolometric luminosity for AGB stars in the solar neighbourhood. The luminosity distribution of nearby AGB stars is very narrow and centred around $L \sim 3000\,{\rm L}_\odot$ (Knauer, Ivezić & Knapp 2001). Since it is very similar to the luminosity function obtained for the much redder bulge stars, it appears that the luminosity function is similar throughout the Galaxy and not very dependent on stellar colour. Owing to this similarity, it is possible to postulate a universal narrow luminosity function and estimate the distance to each star irrespective of its colour and position in the Galaxy. This allows a *direct* study of their Galactic distribution, rather than constraining it indirectly by modelling the number counts versus flux relation.

(iv) All previous studies *assumed* that the number density distribution is separable in z and R. Although the available *IRAS* data appear sufficient to explicitly test this assumption, this has not yet been done. In addition, subsamples of AGB stars with different colours (reflecting different mass-loss rates) can be formed, allowing a study of differences in their Galactic distribution.

In Section 2 we discuss the *IRAS* data and the method developed for selecting AGB stars. The determination of the Galactic distribution of ∼10 000 selected stars is described in Section 3, and in Section 4 we analyse the time evolution of AGB mass loss. The results are summarized and discussed in 5.

2 SELECTION METHOD

2.1 The *IRAS* PSC data

The *IRAS* colour–colour and colour–magnitude diagrams have been used extensively to select and classify various types of dusty star

(e.g. van der Veen & Habing 1988; Walker et al. 1989). Recently, IE00 showed that all *IRAS* sources can be separated into four classes, including AGB stars. They obtain a very clean classification using a scheme that requires at least three *IRAS* fluxes. For AGB stars the three best bands are typically 12, 25 and 60 μm. However, as already pointed out by Habing (1988), the requirement that the *IRAS* flux at 60 μm should be of good quality significantly decreases (by more than a factor of 4) the number of available sources. Furthermore, even for stars with a formally good 60-μm flux, there is significant contamination by interstellar cirrus emission (Ivezić & Elitzur 1995, hereafter IE95). For this reason, we can use only the *IRAS* fluxes at 12 and 25 μm, and the resulting colour $[25]–[12] = \log(F_{25}/F_{12})$.

There are 88 619 sources in the *IRAS* PSC with both the 12- and 25-μm flux qualities greater than 1. Their [25]–[12] colour and F_{12} flux distributions are shown in the top two panels in Fig. 1. The right-hand panel indicates that the sample is complete to $F_{12} \sim 1$ Jy. The left-hand panel shows the colour distribution for 64 329 sources with $F_{12} > 1$ Jy. There are two obvious peaks: at $[25]–[12] = -0.6$, representing stars without dust emission, and at $[25]–[12] = -0.25$, which is dominated by AGB stars (IE00).

The colour and flux distributions of the stars in the sample are very dependent on the Galactic coordinates. The two panels in the second row in Fig. 1 show the colour and flux distributions for a subsample of 1022 stars towards the Galactic poles ($|b| > 60°$) compared with the colour distribution of the whole sample. The

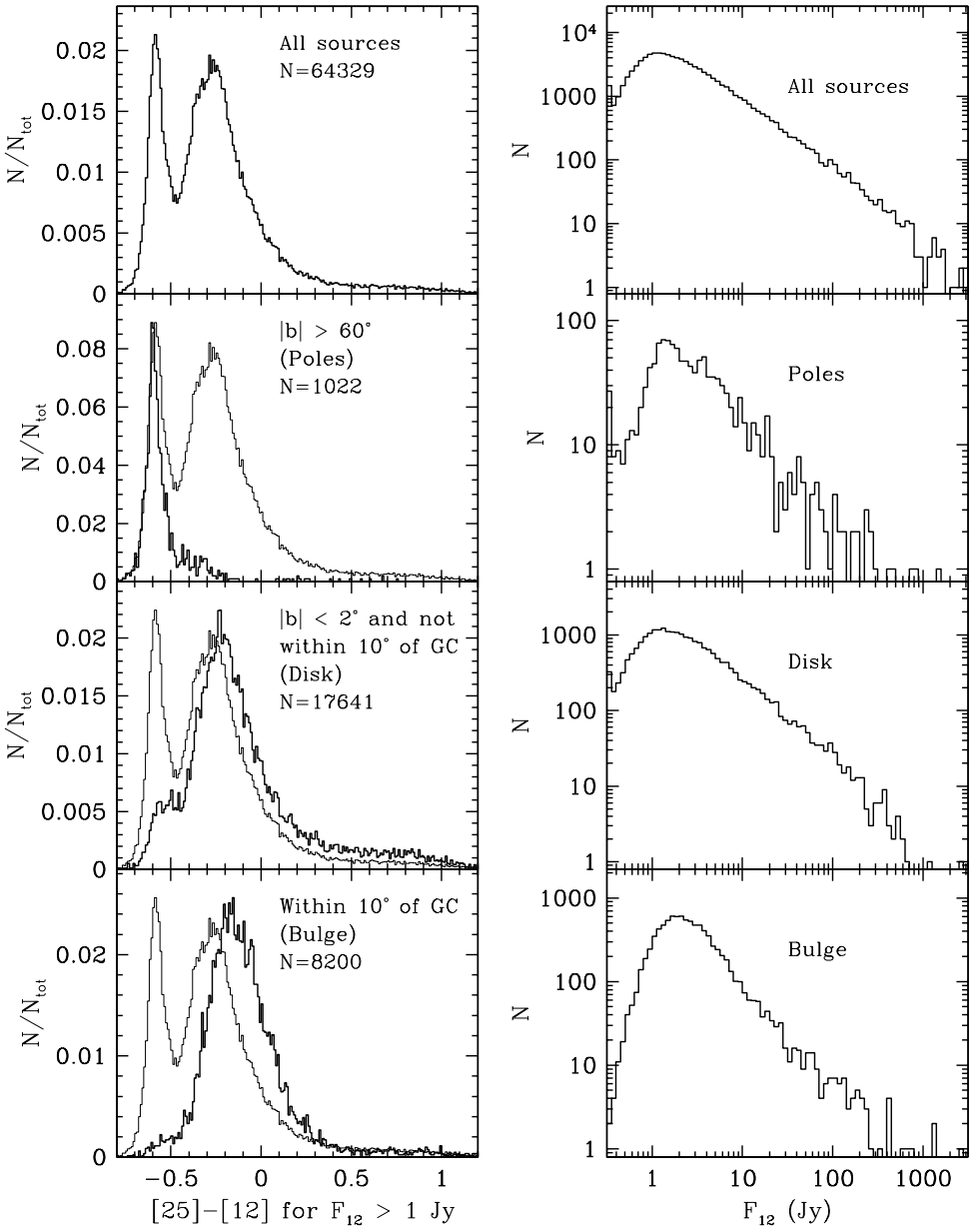

Figure 1. The top two panels show *IRAS* F_{12} flux distributions for the 88 619 sources with both 12- and 25-μm flux qualities greater than 1 (right) and [25]–[12] colour distributions for the subset of 64 329 sources with $F_{12} > 1$ Jy (left). The following three rows show analogous histograms for subsamples selected by their Galactic coordinates, as marked in the panels. Their colour distribution is shown by the thick line, and compared with the colour distribution of the whole sample shown by the thin line.

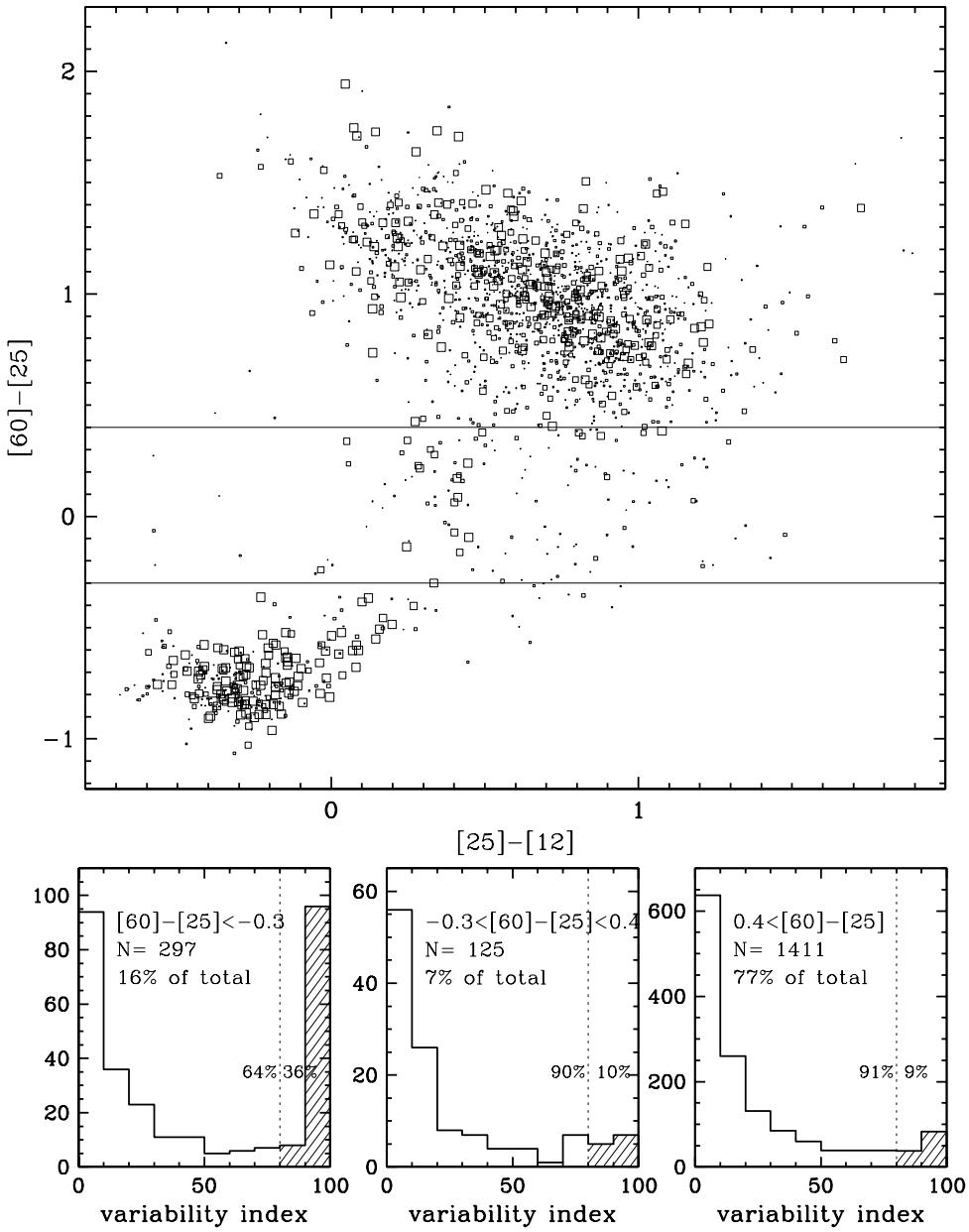

Figure 2. The top panel shows *IRAS* [60]–[25] versus [25]–[12] colour–colour diagram for 1624 sources with both the 12-, 25- and 60-μm flux qualities equal to 3. The symbol size is proportional to the variability index. The bottom panels show the variability index distribution for three subsamples selected by [60]–[25] colour.

high-latitude sample is dominated by dust-free stars, while the disc stars and stars towards the bulge are dominated by AGB stars, as evident in the panels in the last two rows. The strong dependence of the colour and flux distributions on the Galactic position indicates the rich information on the Galactic structure encoded in these data.

2.2 The AGB sample selection criteria

Fig. 2 in IE00 shows that sources with [25]–[12] < -0.2 are dominated by AGB stars, and that their fraction becomes negligible for [25]–[12] > 0.2, where the sample is dominated by young stellar objects. An optimal separation line between the AGB stars and other sources (mostly young stellar objects and planetary nebulae) is [25]–[12] $= 0$. While it is tempting to define the sample by using only this criterion, Blommaert et al. (1993) showed that colour-selected samples may be significantly contaminated by sources other than AGB stars such as pre-main-sequence stars and planetary nebulae. They also pointed out that the *IRAS* variability index, *var*, is a reliable indicator of AGB stars (which are known to vary on time-scales of $\sim$1 yr). This finding was further reinforced by Allen, Kleinmann & Weinberg (1993) who found that the *IRAS* stars with high variability index are dominated by AGB stars.

The *IRAS* variability index was estimated by comparing the number of sources with correlated flux excursions exceeding $m\sigma$ at 12 and 25 μm, $N_c(m)$, with the number of sources showing anticorrelated flux excursions exceeding $m\sigma$, $N_a(m)$, where σ is the measurement error. The probability that a source is variable is computed from

Table 1. The statistics for colour and variability selection cuts (see the text).

[60]–[25]:	<-0.3	-0.3–0.4	>0.4	All
N(total)	297	119	1208	1624
N([25]–[12] < 0)	258	7	28	293
$N(var > 80)$	104	12	110	226
N(selected)	90	0	3	93

$$p = (a - b)/(a + b), \quad (1)$$

where $a = N_c(m)/N_c(0)$ and $b = N_a(m)/N_a(0)$ (IRAS Explanatory Supplement,[2] equation V.H.3). In order to determine an optimal AGB selection cut for the variability index, we investigated the distribution of the variability index, $var = p \times 100$ per cent, in the *IRAS* 12-25-60 colour–colour diagram. Fig. 2 shows the [60]–[25] versus [25]–[12] colour–colour diagram for the 1624 sources with the highest-quality fluxes at 12, 25 and 60 μm. These sources have three reliable fluxes, and thus can be reliably classified by their position in the [60]–[25] versus [25]–[12] colour–colour diagram, as described by IE00. The two horizontal lines divide the diagram into regions dominated by AGB stars ([60]–[25] < -0.3), planetary nebulae ($-0.3 <$ [60]–[25] < 0.4) and young stellar objects ([60]–[25] > 0.4). The number of sources in each region is listed in the first row of Table 1. Sources with a high variability index ($var > 80$) are found throughout the diagram, but at a higher rate among AGB stars. This is better seen in the three histograms shown at the bottom of the figure, where only AGB stars show a strong excess of high variability index, $var > 80$. There are 36 per cent of AGB stars with $var > 80$, while only 10 per cent or less of other sources show such a high variability index.

We adopt $var > 80$, which is the minimum of the var distribution in the whole sample, as the additional selection criterion for AGB stars. According to the *IRAS* Explanatory Supplement (Section VII.D.3), this variability cut roughly corresponds to a variability amplitude of approximately 0.2 mag. The sample of 1624 sources with high-quality fluxes can be used to estimate the selection efficiency. Fig. 3 compares the selection method for three types of source separated by their [60]–[25] colour: all sources, sources with $var > 80$ and those with high variability index and [25]–[12] < 0. The number of sources in each category is listed in Table 1. Only ∼3 per cent of the sample selected by using both the colour and variability criteria are non-AGB stars.[3] This is a significant improvement compared with the sample selected only by colour, which contains ∼12 per cent of non-AGB stars.

The adopted variability cut selects 35 per cent of all AGB stars with [25]–[12] < 0. While using only the colour selection would increase the sample size by almost a factor of 3, the analysis by Habing (1988) and Blommaert et al. (1993) showed that contamination may significantly affect the derived conclusions.

The variability cut, while efficient in excluding non-AGB sources, may introduce a selection bias. For example, the variability detection could be significantly dependent on the colour, flux or position. Indeed, only ∼70 per cent of the sky was surveyed three times during the *IRAS* mission, while 20 per cent was observed only twice, and thus the variable sources in some parts of the sky were more likely to be detected than others. Fortunately for the analysis presented in this paper, the *IRAS* scans were arranged along lines of constant ecliptic longitude, and consequently this effect is not strongly correlated with Galactic structure (we discuss this further in Section 3.5).

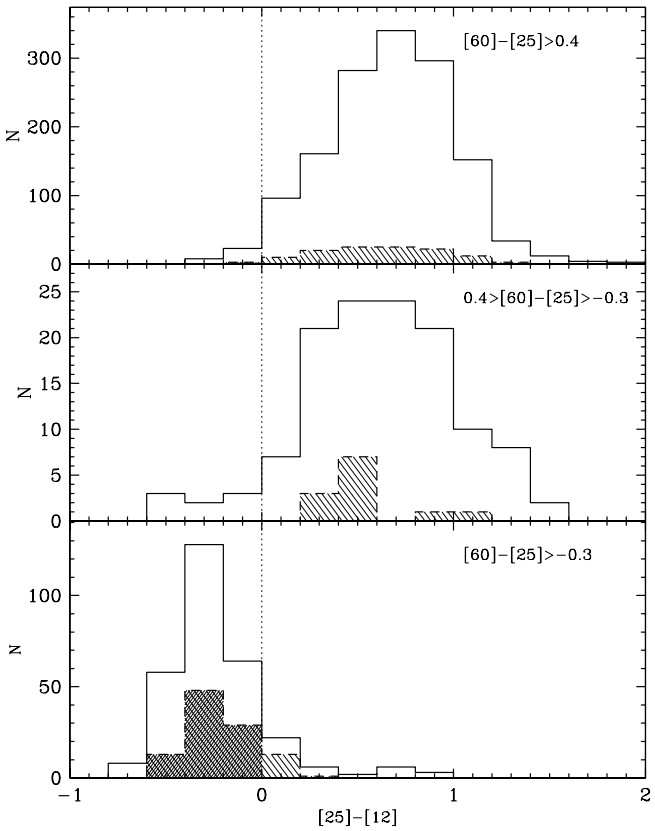

Figure 3. The comparison of the selection methods in three bins of [60]–[25] colour. The solid line shows the (unshaded) histogram of all sources in a given [60]–[25] bin, and the dashed line shows the (hatched) histogram for sources with the variability index greater than 80. The cross-hatched histogram indicates sources with both high variability index and [25]–[12] < 0.

We analyse the possibility of a selection bias with respect to flux and colour by comparing the distributions of the F_{12} flux and [25]–[12] colour for the sample of 293 stars with high-quality fluxes and classified as AGB stars, to the distributions for a subsample of 93 stars with $var > 80$. The top panel in Fig. 4 compares the [25]–[12] colour histogram for the whole sample and for sources with $var > 80$. As is evident, there is no strong dependence of this fraction on colour in the $-0.5 <$ [25]–[12] < 0 range. The bottom panel in Fig. 4 shows the analogous histograms and the corresponding fraction when the sample is binned by F_{12} flux. Again, there is no significant correlation between the fraction of selected sources and the F_{12} flux. It should be noted that the faint limit of this sample is brighter than for the sample shown in Fig. 1 (40 versus 1 Jy) owing to the difference in required flux qualities. Thus, the possibility of selection biases for faint sources cannot be fully excluded.

In summary, we require that the candidate AGB stars have flux qualities at 12 and 25 μm greater than 1, [25]–[12] < 0, and variability index greater than 80. These selection criteria result in a sample of 10 240 stars, with a sample completeness of 35 per cent and contamination by non-AGB stars of ∼3 per cent.

With only two *IRAS* fluxes it is impossible to reliably distinguish stars with silicate dust from stars with carbon dust. It is estimated that ∼5–10 per cent of AGB stars observed by *IRAS* have carbon

[2] The *IRAS* Explanatory Supplement is available at http://space.gsfc.nasa.gov/astro/iras/docs/exp.sup

[3] Following IE00, we assume that all stars with [25]–[12] < 0 and [60]–[25] < -0.3 are AGB stars.

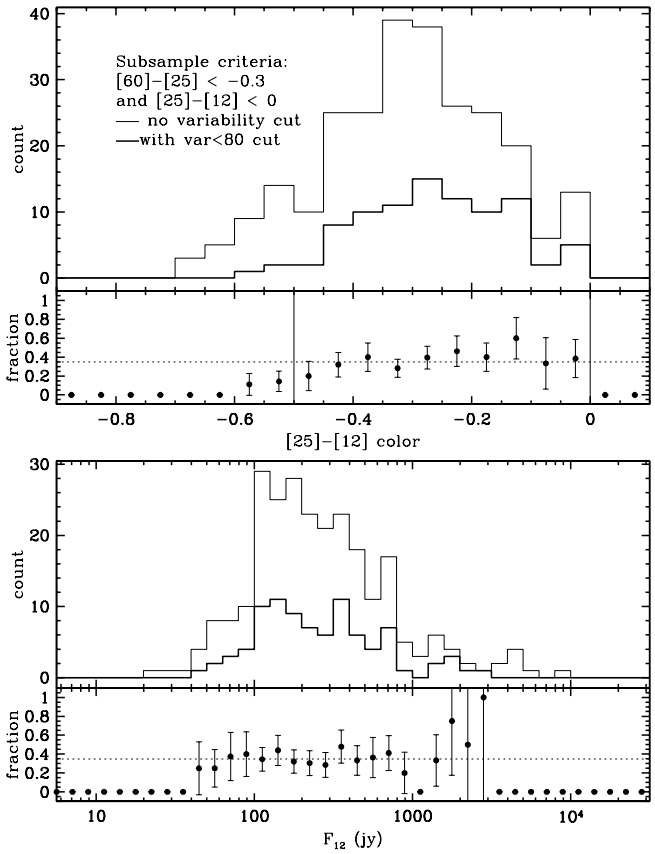

Figure 4. The top panel shows the [25]–[12] colour histogram for the whole sample by the thin line, and for sources with $var > 80$ by the thick line. The symbols show the fraction of the latter in the whole sample for each colour bin. The bottom panel shows the analogous histograms and the corresponding fraction when the sample is binned by F_{12} flux.

dust (e.g. Wainscoat et al. 1992; Whitelock et al. 1994, hereafter WMF94). We adopt 10 per cent for the fraction of carbon stars in the remainder of our analysis.

3 THE GALACTIC DISTRIBUTION OF AGB STARS

Most previous studies utilized number counts as a tool to infer the Galactic distribution of AGB stars (see Section 1). For chosen descriptions of the stellar density distribution and luminosity function, whether in analytic or non-parametric forms, the models are constrained by fitting the predicted counts versus flux relations to the observed counts for different regions on the sky. That is, the Galactic distribution is constrained only *indirectly* through its effect on the observed source counts. Here we follow a different approach: we estimate the distance to each star in the sample and *directly* determine their Galactic distribution.

We estimate distances to individual stars by exploiting the observation that the bolometric luminosity function for AGB stars is fairly narrow, and approximate it by assuming that all stars have the same characteristic luminosity, $L_{\rm AGB}$. Then the distance, D, to a star with bolometric flux, $F_{\rm bol}$, is estimated from $4\pi D^2 = L_{\rm AGB}/F_{\rm bol}$. We utilize the stellar angular distribution towards the Galactic Centre and the known distance to the Galactic Centre, and determine the value of the characteristic luminosity, $L_{\rm AGB}$. By assuming circular symmetry of the Galactic bulge and the disc, we confirm a posteriori that the luminosity function is very narrow.

3.1 The IR bolometric correction for AGB stars

The approach followed here, and in most other studies, depends on a bolometric correction to determine the bolometric (total) flux of star as a function of its measured *IRAS* F_{12} and F_{25} fluxes. It is a standard procedure in the optical wavelength range to use the flux and colour of a star to determine its bolometric flux via

$$m_{\rm bol} = m_1 + BC(m_2 - m_1), \tag{2}$$

where BC is the bolometric correction, m_1 and m_2 are magnitudes at two different wavelengths, and $m_{\rm bol}$ is the bolometric magnitude (e.g. Allen 1973). It is possible to determine the bolometric flux by using only two measurements because stellar SEDs are by and large a function of a single parameter: the effective temperature. While the gravity and metallicity also play a role, their influence on the broad-band fluxes is typically minor ($\lesssim$0.1–0.2 mag, e.g. (Lenz et al. 1998).

It is not clear a priori that an analogous procedure can be used for AGB stars in the IR range. AGB stars have very red SEDs because their stellar radiation is absorbed by a dusty circumstellar envelope and reradiated at IR wavelengths. The SED models for AGB stars typically involve many input parameters (stellar temperature, mass and luminosity, mass-loss rate, dust properties and geometrical dimensions) and it seems that most of them can significantly affect the SED. Nevertheless, it was established empirically that it is possible to construct a well-defined IR bolometric correction for AGB stars (Herman, Burger & Penninx 1986; van der Veen & Rugers 1989). For stars with good photometric wavelength coverage the bolometric flux can be determined by direct integration, and a good correlation is found between the ratio $F_{\rm bol}/F_{12}$ and the [25]–[12] colour, such that

$$F_{\rm bol} = F_{12}\, BC([25]\text{–}[12]), \tag{3}$$

where $BC([25]–[12])$ is the 'infrared' bolometric correction.

The existence of a reasonable IR bolometric correction is understood as a consequence of the scaling properties of the radiative transfer equation, and the universality of the dust density distribution in envelopes around AGB stars (Rowan-Robinson 1980; IE95; Ivezić & Elitzur 1997, hereafter IE97; Elitzur & Ivezić 2001, hereafter EI). While individual parameters such as, for example, the luminosity and the mass-loss rate affect the SED, the SED for given dust grains is fully parametrized by a single parameter, over all optical depth at some fiducial wavelength. Since all dimensionless quantities derived from the SED are functions of the optical depth, including the ratio $F_{\rm bol}/F_{12}$ and [25]–[12] colour, the ratio $F_{\rm bol}/F_{12}$ then must be a function of the [25]–[12] colour. That is, while the effective temperature by and large controls the SEDs of dust-free stars, the SEDs of dust-enshrouded stars are essentially fully controlled by the dust optical depth.[4]

We utilize a bolometric correction derived from the models described in IE95 and computed by the DUSTY code (Ivezić, Nenkova & Elitzur 1997). In particular, we use 'warm' silicate grains from

[4] For optical depths so small that dust emission is negligible, the bolometric correction becomes the bolometric correction of a naked star, which is similar for all such AGB stars because they span a very narrow range of effective temperature. These stars have [25]–[12] < -0.5 and are not included in the final sample discussed here.

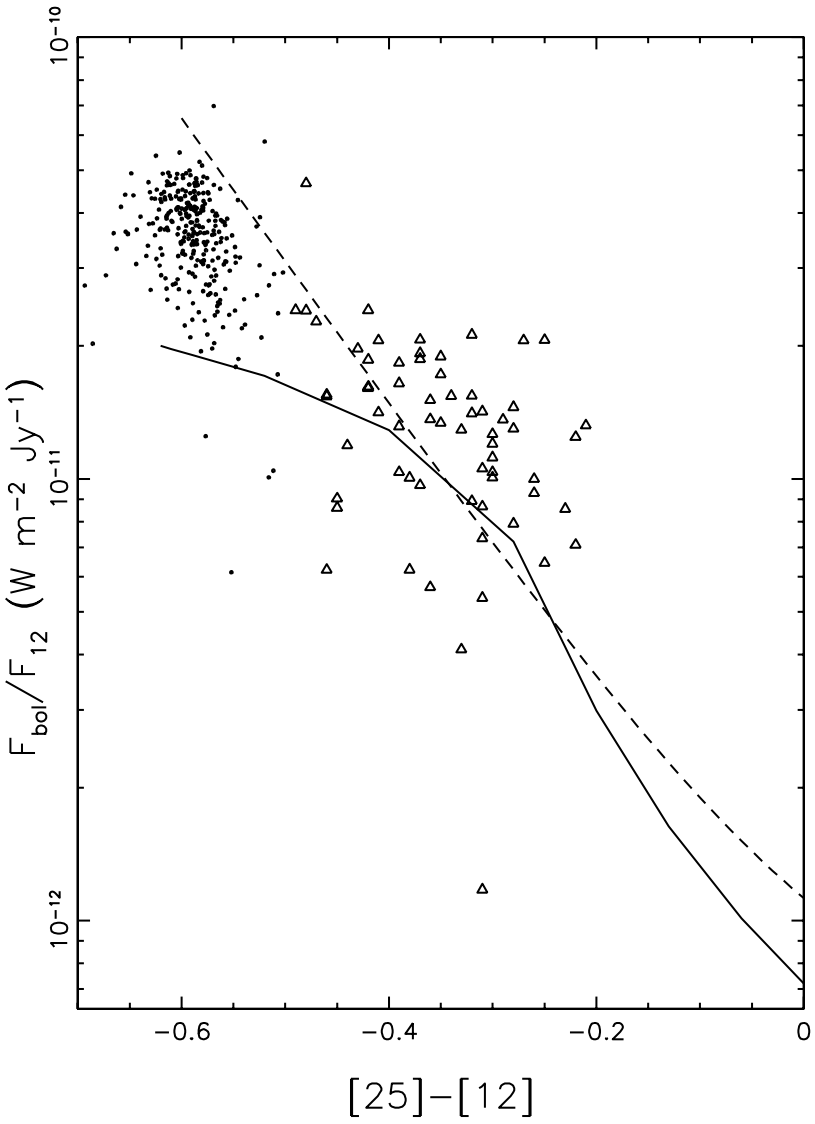

Figure 5. The 'infrared' bolometric correction for AGB stars. The symbols show data for dusty (triangles) and dust-free (dots) stars. The solid line is a model-derived bolometric correction used in this work, and the dashed line is a fit used by van der Veen & Breukers (1989).

Ossenkopf, Henning & Mathis (1992), assume that stellar spectrum is a 3000-K blackbody and that the highest dust temperature is 500 K. These values provide the best agreement with the data discussed by Knauer et al. (2001), and shown as symbols in Fig. 5. For comparison, we show the bolometric correction determined by van der Veen & Breukers (1989), for a different sample of AGB stars, as a dashed line.

For negligible optical depths ([25]–[12] ~ -0.6) the bolometric correction has the value corresponding to the input stellar spectrum. This value varies with the stellar temperature as T^{-3} because the *IRAS* wavelengths are in the Rayleigh–Jeans domain. As the optical depth increases, the SED is shifted towards longer wavelengths, the ratio of the F_{12} flux and bolometric flux increases (i.e. BC decreases) and the [25]–[12] colour becomes redder. Note that for a given F_{12} the corresponding bolometric flux decreases as the [25]–[12] colour becomes redder. The best-fitting value for the highest dust temperature is approximately 200 K lower than usually assumed when modelling the SEDs of AGB stars. However, this low value is in agreement with Marengo, Ivezić & Knapp (2001) who show that AGB stars (with silicate dust) showing semiregular variability require models with somewhat lower dust temperatures ($\sim$300 K) than stars exhibiting Mira-type variability ($\sim$750 K).

We conclude that it is possible to use IR bolometric correction for AGB stars to estimate their bolometric fluxes from *IRAS* F_{12} and F_{25} fluxes, albeit with an uncertainty of up to a factor of 2. We show below that the actual uncertainty in derived bolometric fluxes seems to be not larger than $\sim$50 per cent.

3.2 Determination of $L_{\rm AGB}$

By assuming that all AGB stars have the same luminosity, $L_{\rm AGB}$, and adopting a model-derived bolometric correction, the distance to each star is estimated from

$$D = \left[\frac{L_{\rm AGB}}{4\pi F_{12}\, BC([25]–[12])} \right]^{1/2} . \quad (4)$$

The characteristic luminosity, $L_{\rm AGB}$, is, of course, unconstrained in the case of an individual star without an independent distance

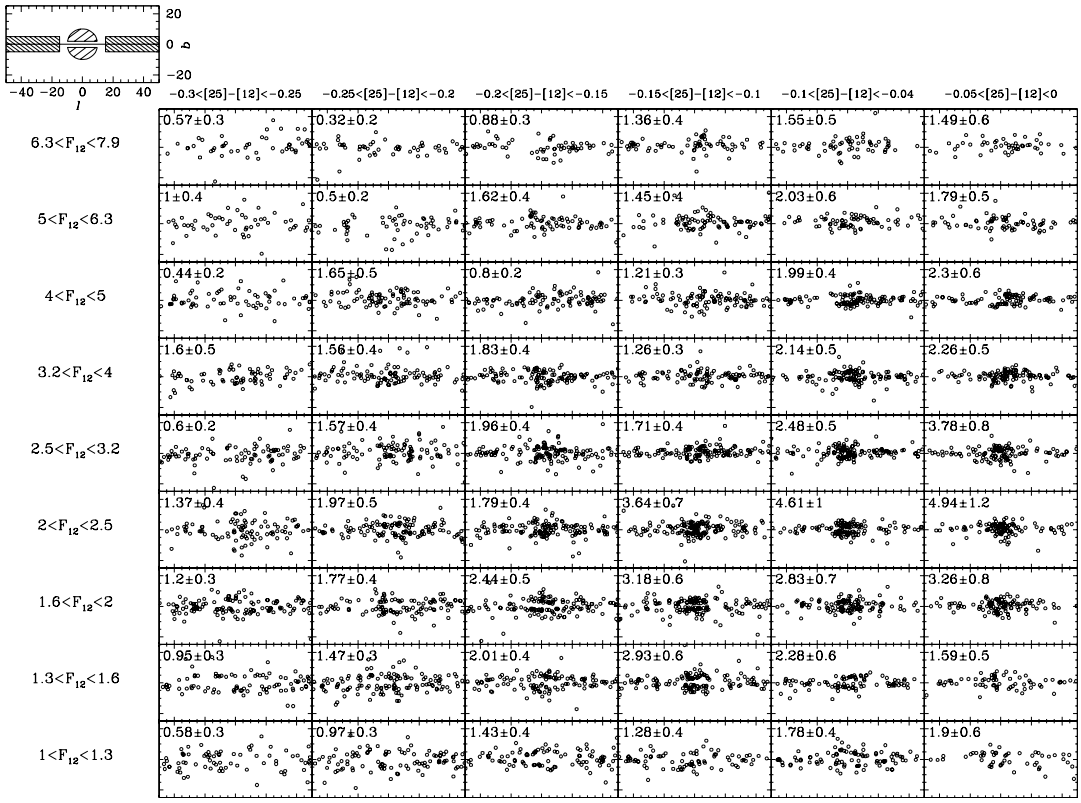

Figure 6. The angular distribution of stars selected by the F_{12} flux and [25]–[12] colour. The numbers show the bulge-to-disc counts ratio in each bin for stars selected by using angular masks shown in the upper left-hand corner.

estimate. Nevertheless, $L_{\rm AGB}$ can be estimated for an *ensemble* of stars because the stellar distribution has a local maximum at the Galactic Centre, and the distance to the Galactic Centre is well determined (we use 8 kpc, Reid 1989).

As shown by Habing et al. (1985), 'properly' colour-selected *IRAS* point sources clearly outline the Galactic disc and the bulge. This observation unambiguously indicates that *IRAS* observed AGB stars as far as the Galactic bulge; however, it is not clear what is the limiting distance to which *IRAS* detected AGB stars. The incompleteness effects close to the faint sensitivity limit may bias the estimate of $L_{\rm AGB}$.

We examined this limiting distance by a method that does not depend significantly on the sample completeness near the faint cut-off. We compare the counts ratio of stars seen directly towards the bulge, and disc stars (both selected by applying angular masks, see below) selected from narrow colour and flux bins. Since both subsamples have the same observed flux, they are affected by incompleteness in a similar way. Similarly to the number counts, the number counts *ratio* of the two subsamples is also expected to show a local maximum corresponding to stars 8 kpc away. Thus, finding the flux–colour bin that maximizes the bulge-to-disc counts ratio determines the bolometric flux of stars at the Galactic Centre, and consequently $L_{\rm AGB}$. The power of the method stems from the fact that the incompleteness effects nearly cancel out because a ratio of counts is taken.

The candidate bulge stars are selected as those within a circle coinciding with the Galactic Centre and a radius of 10°, except those with $|b| < 2^\circ$, which are excluded because of confusion. The mask for the disc star sample is defined by $|b| < 5^\circ$ and $15^\circ < |l| < 50^\circ$.

We define 60 bins[5] in the F_{12} versus [25]–[12] plane, and for each determine the bulge-to-disc star count ratio (the colour is limited to >-0.3 because bluer stars are not detected all the way to Galactic Centre, see below). Fig. 6 shows the angular distribution of stars in these bins. The bulge and disc masks are shown in the upper left-hand corner. It is evident that the count ratio varies greatly among the bins, and has values indicating both bulge detection (>1) and non-detection (~ 1). For each colour bin there is a local maximum of the count ratio corresponding to the stars at the Galactic Centre. The count ratio decreases for fainter F_{12} flux because stars in those bins are behind the Galactic Centre.

The behaviour of the bulge-to-disc count ratio is easier to discern if shown in the $F_{\rm bol}$ versus [25]–[12] plane. Fig. 7 displays information similar to Fig. 6, except now the counts ratio is shown by different shades: the darkest for >3, medium for 2–3, and the lightest for 1–2 (the bin boundaries are no longer rectangular because $F_{\rm bol}$ is used instead of F_{12}). The highest contrast is obtained for bins with [25]–[12] $\gtrsim -0.2$ and for $F_{\rm bol} = 1.9 \times 10^{12}$ W m^{-2}. In principle, the highest contrast for each colour bin should be obtained at the same value of $F_{\rm bol}$. As is evident from the figure, the bluer bins appear to

[5] The largest distance at which an AGB star could be observed is strongly colour dependent because the relationship between their characteristic luminosity, $L_{\rm AGB}$, and observed flux, F_{12}, includes the colour-dependent bolometric correction. For example, for $L_{\rm AGB} = 3500$ L$_\odot$ and $F_{12} = 1$ Jy, stars with [25]–[12] = 0 can be seen to ∼14 kpc, while stars with [25]– 12] = −0.4 only to ∼3 kpc. This effect mandates that the analysis is performed for colour ranges sufficiently narrow that the bolometric correction is approximately constant. Given the sample size and the behaviour of the bolometric correction, we find that 0.05 is a good choice for the colour bin size.

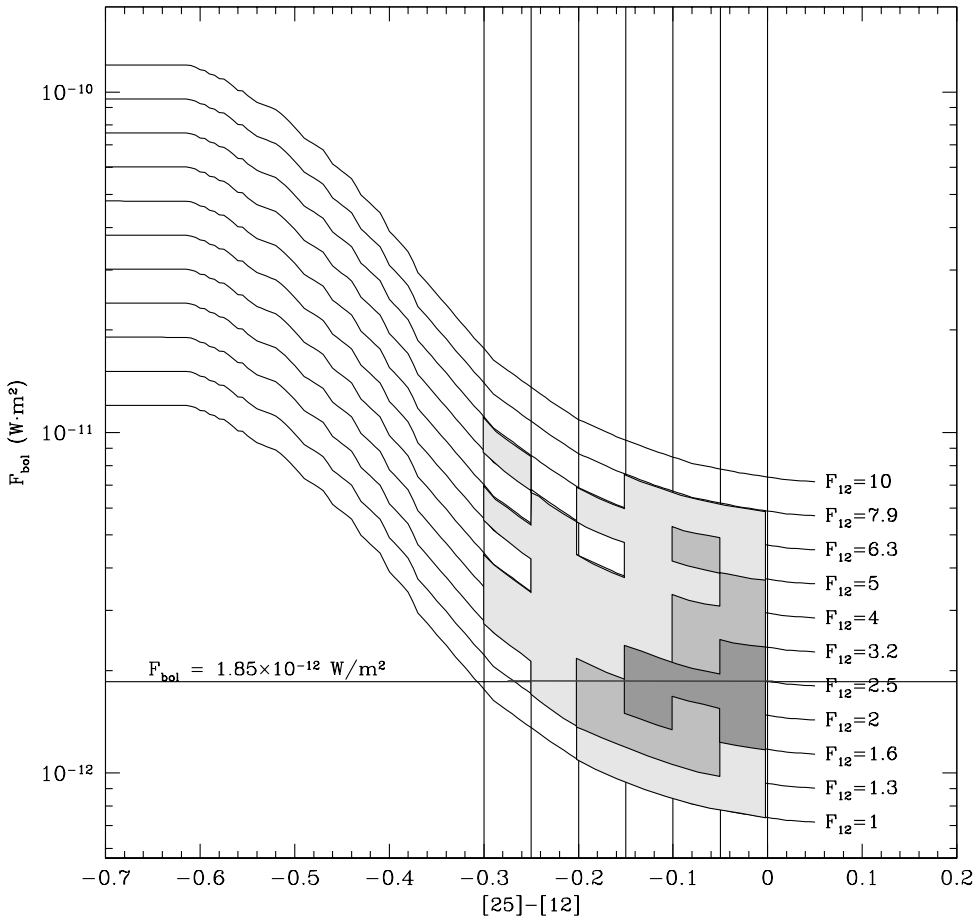

Figure 7. The bulge-to-disc count ratio in the $F_{\rm bol}$ versus [25]–[12] plane. The counts ratio is shown by different shades: the darkest for >3, medium for 2 to 3, and the lightest for 1 to 2.

imply an $F_{\rm bol}$ larger by approximately a factor of 2. However, the blue bins corresponding to $F_{\rm bol} = 1.9 \times 10^{12}$ W m^{-2} have F_{12} very close to the sample completeness limit at $F_{12} \sim 1$ Jy: so close to the sample faint limit that even the 'counts ratio' method falls apart, and the apparent bias in $F_{\rm bol}$ for blue bins cannot be interpreted as a real effect. We adopt $F_{\rm bol} = 1.9 \times 10^{12}$ W m^{-2} as the bolometric flux of an AGB star at the Galactic Centre, implying $L_{\rm AGB} = 3500$ L$_\odot$ for a distance to the Galactic Centre of 8 kpc. This value could be uncertain by as much as a factor of 2, and we estimate its probable uncertainty below.

3.3 Optimal bulge selection

Based on the above discussion, in particular on the results presented in Fig. 6, we can optimize the bulge selection criteria to minimize contamination. In essence, the F_{12} versus F_{25} plane is mapped on to the distance–colour plane, and requiring a distance range of, for example, 7–9 kpc simply means defining a corresponding region in the F_{12} versus F_{25} plane (or, equivalently, the F_{12} versus [25]–[12] plane). We find that selecting stars with $1.25 < F_{12}/$ Jy < 3.0 and $-0.17 <$ [25]–[12] < 0.0 produces a bulge-to-disc contrast ratio of ∼3. While this is lower than the maximal possible ratio (e.g. ∼5 for $2 < F_{12}/$ Jy$^{-1} < 2.5$ and $-0.05 <$ [25]–[12] < 0, see Fig. 6.) the relaxed criteria produce a much larger sample (1710 instead of 231 stars) The bulge-to-disc contrast ratio of ∼3 is still larger than the ratio obtained by following the prescription from Habing et al. (1985), which produces a contrast of 1.6 (albeit with a much larger sample). The angular distributions of stars selected by these two criteria are compared in the two top panels in Fig. 8.

One of the reasons why the above selection produces a larger bulge-to-disc contrast than the sample of Habing et al. is that their sample contains disc stars that are in front of the bulge and behind the bulge, but are observed towards the bulge. The results from Fig. 6 can be used to select such stars, too. The third and the fourth panels in Fig. 8 show the angular distribution of stars in front of the bulge and behind the bulge, selected from the sample of Habing et al. Another reason for the lower contrast is that their sample is probably contaminated by non-AGB stars. This contamination would be large for [25]–[12] > 0, and the bottom panel in Fig. 8 shows the angular distribution of such stars. Their bulge-to-disc count ratio is only 1.25.

3.4 Determination of the width of the luminosity function

With the assumption of a constant luminosity of 3500 L$_\odot$, and with the bolometric correction shown in Fig. 5, it is straightforward to calculate the distance for each star. We assume that the extinction is 0.030 mag kpc^{-1} at 12 μm and 0.015 mag kpc^{-1} at 25 μm, resulting in corrections for stars at the Galactic Centre of 25 per cent for the flux and Δ ([25]–[12]) = 0.05 for the colour (in order to minimize incompleteness effects, we require $F_{12} > 1$ Jy). This is the faintest flux limit that still allows the detection of stars at the Galactic Centre,

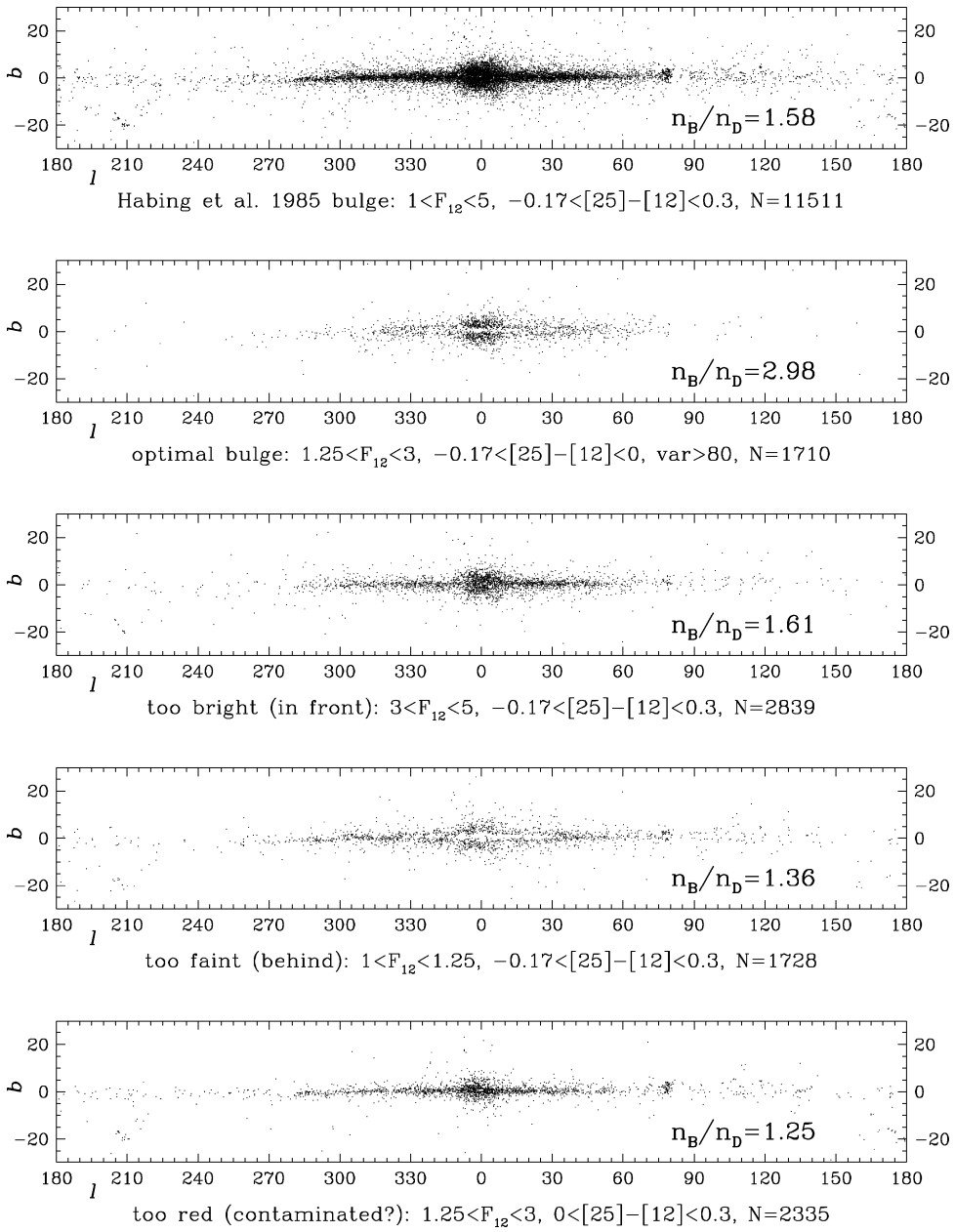

Figure 8. The angular distribution of stars selected by various cuts based on the F_{12} flux and [25]–[12] colour. The numbers show the bulge-to-disc counts ratio.

and results in a sample of 9926 stars. This limit also guarantees that the sample is not affected by the *IRAS* faint limit at 25 μm. In order to visualize the dependence of the Galactic distribution of AGB stars on their [25]–[12] colour, we divide the sample into the 'blue' subsample with [25]–[12] < -0.25 (3352 stars), and the 'red' subsample with [25]–[12] > -0.25 (6574 stars).

Fig. 9 shows the three Cartesian projections of the Galactic distribution of stars in the red subsample. The *X*–*Y* and *X*–*Z* panels indicate that the sample extends beyond the Galactic Centre. It is visible in the *X*–*Z* panel (upper right-hand corner) that the limiting distance for stars beyond the Galactic Centre depends on the height above the Galactic plane. Stars close to the plane are observed through the bulge, and these lines of sight have a somewhat higher faint cut-off caused by the source confusion (this effect is *not* caused by interstellar extinction).

The stars appear to trace out a bar-like structure of length ∼5 kpc pointing towards the Sun, but this is an artefact of the assumption that all stars have the same luminosity. Since the true luminosity function must have a finite width, we can estimate this width by assuming a spherical bulge.

By analysing the counts of stars in two strips 2 kpc wide parallel to the *X* and *Y* axes, we find that the equivalent Gaussian width of the start count histogram along the *X* axis is between 1.5 and 2.5 times as large as along the *Y* axis (1.2–2.0 kpc versus 0.8 kpc). The histogram width along the *X* axis is harder to measure than the width along the *Y* axis because it is not fully symmetric around $X = 0$ caused by the incompleteness effects behind the Galactic Centre. We conservatively adopt 2 kpc for the effective widening of the stellar distribution caused by a finite width of the luminosity function, which implies that the scatter (the equivalent Gaussian

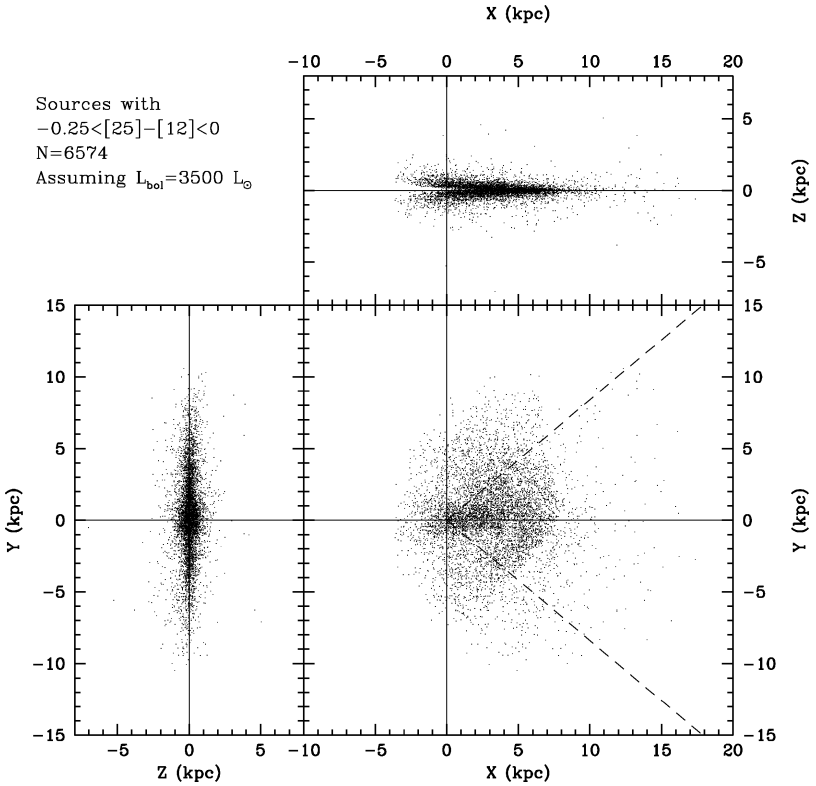

Figure 9. The Galactic distribution of AGB stars with $-0.25 < [25]–[12] < 0.0$, where each star is shown as a dot. The Sun is located at ($X = 8$ kpc, $Y = 0$, $Z = 0$).

width) of luminosity about the mean value is approximately a factor of 2. In other words, the majority of stars (66 per cent) have their bolometric luminosity between 2000 and 7000 $L_\odot$. The assumption that all stars have the same luminosity smears their distribution such that fine details (such as spiral arms) cannot be recovered.

It was pointed out by the referee that the luminosity distribution obtained here should be compared with other estimates, e.g. to the distribution expected from the period–luminosity relation and period distribution for AGB stars (Feast et al. 1989). The median period for Miras discussed by WMF94 is approximately 300 d, with the scatter of approximately 100 d (their fig. 8). Using the period–luminosity relation from the same paper (equation 2), we find that the implied distribution of bolometric luminosity is centred on 5800 $L_\odot$, with a scatter of approximately 50 per cent. This is in good agreement with our results, given the entirely different methods used to derive the two luminosity distributions. Furthermore, the bias in the mean luminosity of ∼0.5 mag (5800 versus 3500 $L_\odot$) is not important for the Galactic distribution of AGB stars discussed in subsequent sections because all distances in this paper are tied to the distance to the Galactic Centre.

Fig. 10 shows the Galactic distribution of stars in the blue subsample. For the same bolometric flux these stars have fainter *IRAS* fluxes than stars in the red subsample, and consequently a shorter limiting distance. As evident from the figure, these stars are *not* observed all the way to the Galactic Centre.

3.5 Analysis of the Galactic distribution of AGB stars

The Galactic distribution of AGB stars (using the luminosity function discussed above, $L_{\rm AGB} = 3500\ L_\odot$) in Figs 9 and 10 shows jumps in the number density along the lines of sight defined by $l \sim 70^\circ$ and 320°. Both features are data artefacts. The first jump happens at the intersection of the *IRAS* missing data region with the Galactic plane (the so-called 5° gap, see the *IRAS* Explanatory Supplement, Section III.D). The other jump at $l = 320^\circ$ only shows up after the variability cut ($var > 80$). This feature (and other more subtle structures) is a sampling effect because in this region the source density is high and the survey strategy produced extra scans at time intervals suitable for detecting variability.

In order to minimize these effects, and to study a well-defined volume, we further limit the sample to a wedge starting at the Galactic Centre, symmetric around the X axis, and with an opening angle of 80°. Its boundaries are shown by dashed lines in Figs 9 and 10. This constraint leaves 6804 stars in the sample. While the applied restriction does not completely remove these features, it allows for a robust determination of the source distribution inside the solar circle and several kpc beyond it. However, around $R \sim 8$ kpc any local features in the number density should be treated with caution. These two instrumental effects should not produce any bias in the z-direction, and are presumably not dependent on colour.

3.6 The non-parametric estimates

The sample remaining after all selection cuts is still large enough to explicitly test the hypothesis that the Galactic distribution of AGB stars is separable in Galactocentric distance, R, and distance from the Galactic plane, z. If so, then the vertical (z) distributions in different radial (R) bins should be statistically indistinguishable (apart from the normalization factor). We also separate the stars by colour into several subsamples in order to constrain the relationship between the colour and the Galactic distribution.

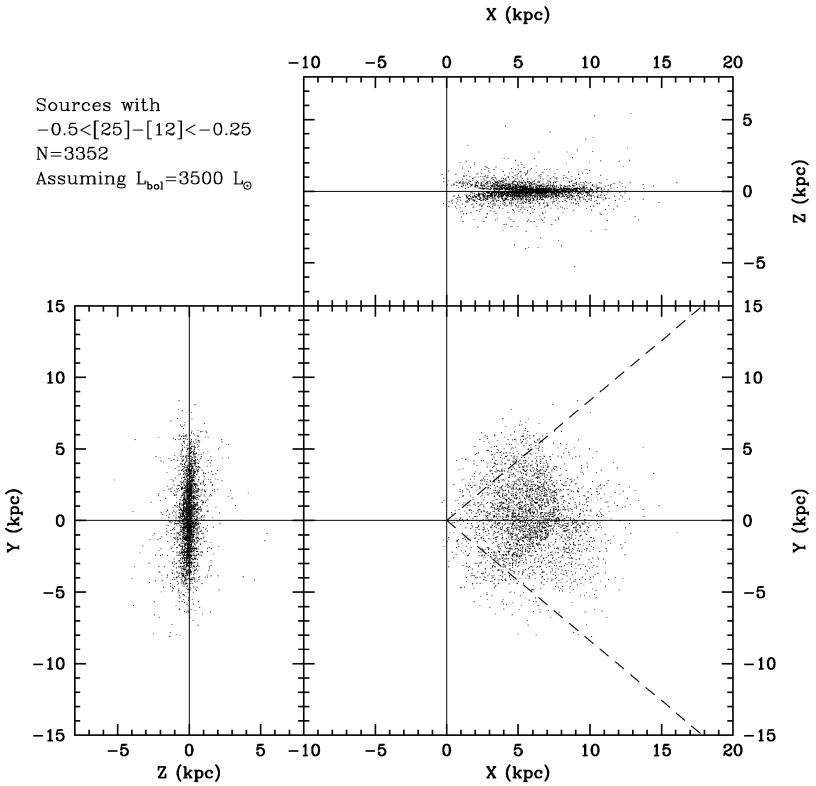

Figure 10. The same as in the previous figure, except that $-0.50 < [25]–[12] < -0.25$.

3.6.1 The vertical z distribution

Fig. 11 displays the z distributions, shown as histograms with error bars, for three colour subsamples (the [25]–[12] colour in the ranges −0.5 to −0.3, −0.3 to −0.15 and −0.15 to 0), and in three radial ranges (2–5, 5–8 and 8–12 kpc), starting with the top left-hand panel. The small numbers show the number of stars in each bin (these counts are not corrected for the selection efficiency of ∼35 per cent, see Sections 2.2 and 3.8). Since all histograms are well described by an exponential function,

$$n(z) = n_0 \mathrm{e}^{-|z|/h_z}, \quad (5)$$

we determine its scaleheight, h_z, by fitting the counts for $|z| < 1.5$ kpc. The number of stars in each subsample (N) and the best-fitting scaleheights are shown in each panel. The scaleheights vary from 226 to 381 pc, with marginal evidence ($\sim 3\sigma$) that the scaleheight decreases with [25]–[12] colour. While a 3σ effect may appear significant, we emphasize that the error bars are simply based on Poisson statistics, and do not include any systematic effects. A similar level of significance is obtained for the correlation between the best-fitting scaleheight and the radial direction, where the last radial bin appears to have a somewhat larger scaleheight (as in, for example, a flared disc).

To test further whether the data support these correlations, we determine the best-fitting scaleheight for the whole sample, i.e. without the radial and colour binning, and compare it with each subsample. The bottom right-hand panel in Fig. 11 shows the z distribution for the whole sample as a histogram, and the best exponential fit by a thin solid line. The same exponential fit (for the whole sample) is then compared with each subsample in the other three panels, and is shown as a thin solid line. We include only points with $z < 1.5$ kpc where the signal-to-noise ratio is the highest, and use the same weight for all points. As is evident, the total sample scaleheight of 286 ± 10 pc is not obviously inconsistent with the distribution of each subsample (while formally the χ^2 per degree of freedom is somewhat larger than 1, the unknown systematic errors may account for the variation of scaleheight among the subsamples). We conclude that there is no compelling evidence that the scaleheight depends significantly on the [25]–[12] colour or the Galactocentric distance.

The histogram shown in the bottom right-hand panel of Fig. 11 is systematically above the best-fit exponential for $|z| \gtrsim 1.5$ kpc. This excess of counts appears consistent with the thick disc proposed by Gilmore & Reid (1983). However, this discrepancy has no statistical significance; the number of stars in all radial bins with $|z| > 1.5$ kpc is 101, or ∼1.4 per cent of the total number of stars, comparable to the estimated 3 per cent sample contamination by non-AGB stars (see Section 2.2). Such contaminants are dominated by stars with luminosity much smaller than the adopted AGB luminosity (3500 $L_\odot$). While there is growing support for the thick disc (e.g. Chen et al. 2001 and references therein), its existence is *not* required by the *IRAS* counts of AGB star candidates.

The dashed and dotted lines in the bottom right-hand panel of Fig. 11 show two fits of the sech^2 function. This function was proposed by Habing (1988) to be a better description of the z distribution of AGB stars than a simple exponential function, and was utilized to model the *IRAS* counts. The dashed line is a best fit that reproduces the observed counts at $z \approx 0$. However, it falls off too fast for $z \gtrsim 1$ kpc. The dotted line produces a good fit (to the exponential best fit) for large z, but significantly underestimates the counts for $z = 0$. We conclude that a simple exponential function is a much better description of the z distribution of selected AGB star candidates than the sech^2 function for $z < 1.5$ kpc. This conclusion is in agreement with Kent, Dame & Fazio (1991) who analysed a 2.4-μm map of the northern Galactic plane.

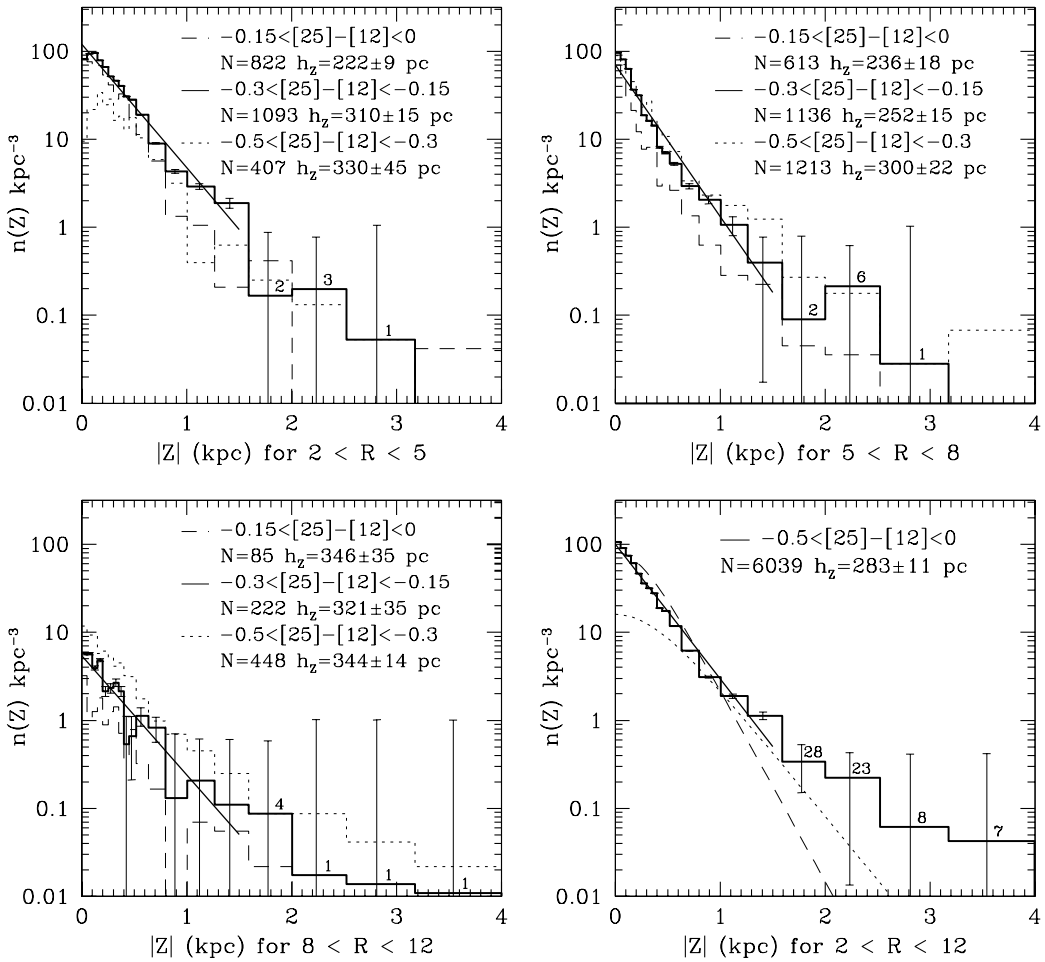

Figure 11. The distribution of selected AGB star candidates perpendicular to the Galactic disc. An exponential fall-off with the scaleheight of 286 ± 10 pc provides a good fit irrespective of the Galactocentric distance, R, and the [25]–[12] colour (see the text).

3.6.2 The radial R distribution

The radial distribution of selected AGB candidates is shown in Fig. 12. The first five panels, starting in the upper left-hand corner, show the R histograms for subsamples binned by the [25]–[12] colour. As was already evident in Fig. 10, the blue subsamples ([25]–[12] $\lesssim -0.3$) do not extend all the way to the Galactic Centre.

The decrease of number density for $R \gtrsim 5$ kpc seems consistent with an exponential fall-off, and each panel displays the best-fitting scalelength obtained for points with $R > 5$ kpc (except for the bluest bin where the limit is $R > 6.5$ kpc). The corresponding fit is shown by a straight line. The number of stars in each colour-selected subsample is also shown in each panel. Note that there are no obvious jumps in the counts at $R \sim 8$ kpc, indicating that selecting the stars within the wedge described in the previous section removes the instrumental effects seen in Figs 9 and 10.

The best-fitting scalelengths span the range from 1.2 to 1.8 kpc, with a typical uncertainty of 0.1 kpc, and the mean value of 1.44 kpc. The bottom right-hand panel shows the histogram for the whole sample (i.e. without the colour binning); its best-fitting scalelength is 1.6 ± 0.07 kpc, consistent with the above mean value.

The counts of stars in the red subsamples ([25]–[12] $\gtrsim -0.2$) increase towards the Galactic Centre for $R < 3$–4 kpc. This increase is caused by the bulge contribution. We do not attempt to fit any analytic function because the resulting fit would be strongly affected by the errors in the adopted luminosity function; that is, the detailed dependence of the counts for $R < 4$–5 kpc cannot be determined. Nevertheless, based on the counts for the subsample with $-0.2 <$ [25]–[12] < -0.1, it appears that the disc contribution for the inner 4–5 kpc may be much flatter than its exponential fall-off inferred for larger R. Based on the analysis presented in Section 3.2, the bulge contributes at least three times as many stars as the disc for $R = 0$. This implies that the disc contribution is roughly constant within the inner $\sim$5 kpc. The counts for the reddest subsample are also consistent with this conclusion.

3.7 A simple model for the Galactic distribution of AGB stars

The Galactic distribution of AGB stars determined in the previous section is only marginally inconsistent with a universal,[6] colour-independent function that appears separable in R and z. The z distribution is well described by an exponential function with the scaleheight of $\sim$290 pc. The R distribution has an exponential fall-off with the scalelength of $\sim$1.6 kpc for $R > 5$ kpc. Within the inner 5 kpc, the counts can be described by a flat component caused by the disc, and a bulge component that increases towards the Galactic Centre.

[6] The Galactic distribution of AGB stars can depend on other observables, e.g. periods.

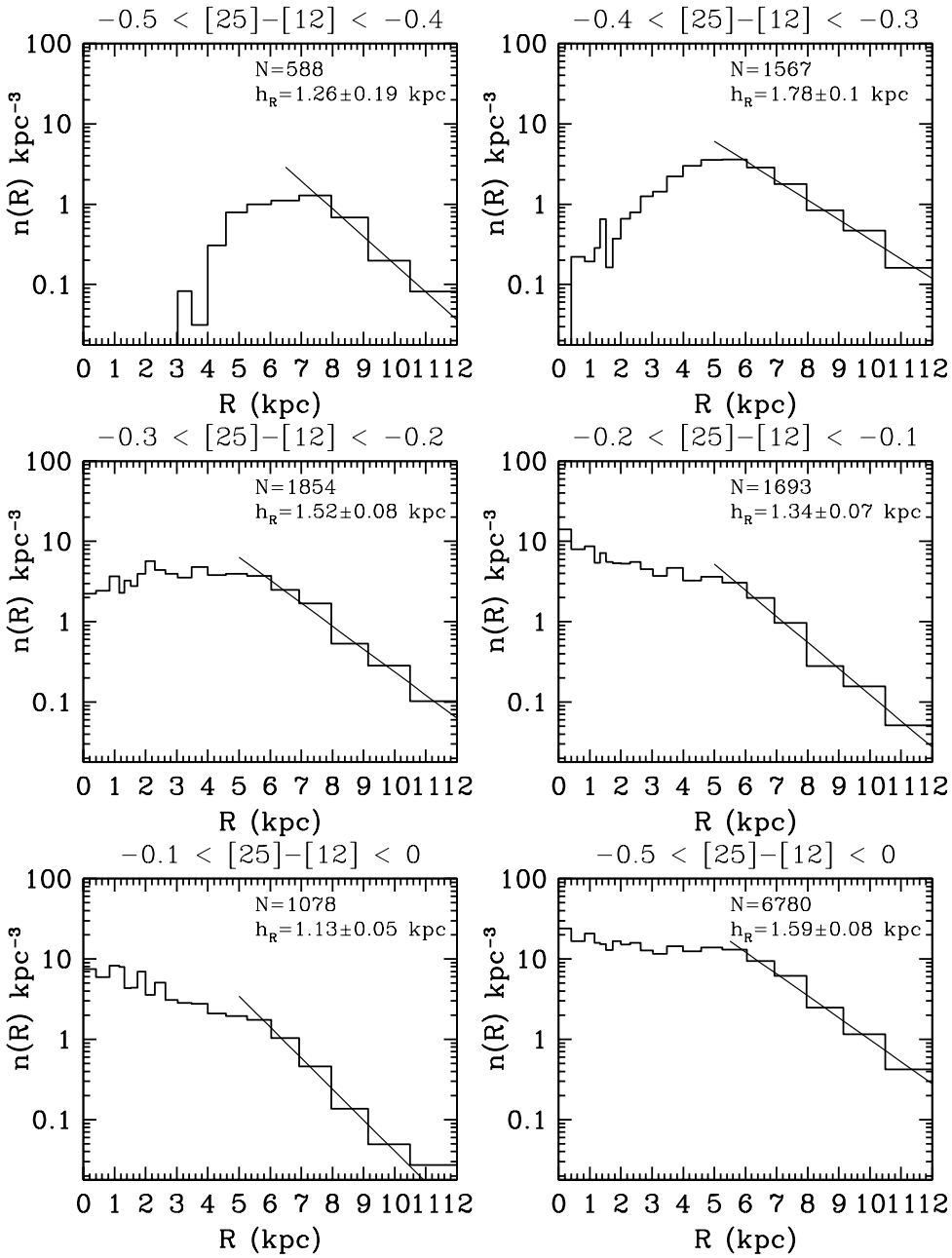

Figure 12. The radial dependence of the AGB star number density.

These results do not vary strongly with the [25]–[12] colour. To illustrate this further, the three panels in Fig. 13 show the dependence of best-fitting scaleheight, scalelength and the number density on colour. This figure can be considered as a summary of results presented in Figs 11 and 12. The error bars are formal uncertainties of the fits and do not include the contributions from the sample contamination and various incompleteness effects. Because these contributions cannot be easily quantified, the displayed results may be interpreted in two different ways.

Formally, it seems that both the scaleheight and the scalelength decrease with [25]–[12] colour. Since the scaleheight decreases with the stellar mass (e.g. Allen 1973), this is consistent with the hypothesis that the mass-loss rate (which by and large controls the [25]–[12] colour, see the next section) increases with stellar mass (see e.g. Habing 1996). The dependence of the scalelength on colour, if real, implies that the high-mass stars are more concentrated towards the Galactic Centre than the low-mass stars. Such a conclusion would be in agreement with the studies of star formation inside and outside the solar circle (Wouterloot et al. 1995; Casassus et al. 1999).

On the other hand, the statistical significance of the possible correlation between the Galactic distribution of AGB stars and their [25]–[12] colour is small. Since there are additional unknown systematic errors, a simple universal description of the Galactic distribution cannot be strongly ruled out. Such a simple description of the distribution of AGB stars, if able to reproduce the data, would be of great value for modelling the Galaxy, and for modelling other galaxies. In order to estimate how well this model would describe the *IRAS* data we perform the following test. We assume a colour-independent Galactic distribution of AGB stars as described at the beginning of this section. The bulge is assumed to follow an

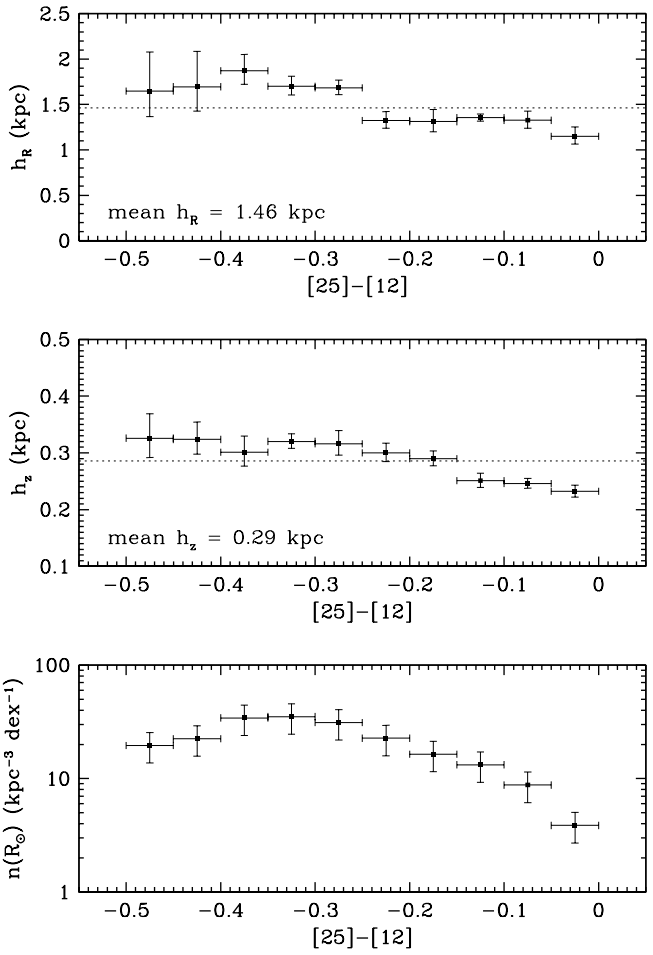

Figure 13. The dependence of the scaleheight and length on colour.

exponential profile with a scalelength of 0.8 kpc (the precise form of the bulge profile is not important since it is not well constrained by the data) with the bulge-to-disc number ratio of 2 at $R = 0$. Utilizing the constant-luminosity $L_{\rm AGB} = 3500\ {\rm L}_\odot$, we generate the model number counts as a function of position on the sky, the F_{12} flux and the [25]–[12] colour for 100 randomly generated samples. The counts depend on the colour despite the colour-independent distribution of stars because of the colour-dependent limiting distance. The discrepancy between this model and the data illustrates the significance of the deviations from the simplified model (this test, of course, does not reveal systematic errors, such as, for example, the sample contamination).

Fig. 14 is reminiscent of Fig. 1 and shows the comparison of the data and the simplified model. The data are shown as squares with Poisson error bars, and the model results are shown by lines. The overall normalization of the model is determined by requiring the same total number of sources as in the data sample. The completeness function at the faint end is determined by requiring the agreement between the data and model counts for the whole sample (that is, the data and the model are forced to agree in the top right-hand panel). The real test of the model lies in the remaining panels where the data and the model are compared for different lines of sight *without* further model adjustments. The overall features in the colour and flux distributions are reproduced fairly well, although there are some formally significant disagreements. While these disagreements illustrate the errors introduced by applying the simplified model, they do not appear sufficient to rule it out.

We used the same modelling approach to test whether the luminosity scatter of 50 per cent introduces a bias in the parameters describing the density distribution. We generated the Galactic distribution of stars according to the best-fitting model discussed above, and computed the 'observed' fluxes by drawing luminosity from a Gaussian distribution centred on $L = 3500\ {\rm L}_\odot$, with the dispersion ranging from of 50 per cent to a factor of 3. Applying an analysis identical to that used for real data we found that the model parameters are reproduced with a bias much smaller ($\sim$3 per cent) than the claimed accuracy of the best-fitting parameters ($\sim$10 per cent) for the luminosity dispersion of 50 per cent. A bias of 10 per cent, comparable to the formal errors of the best-fitting parameters, is obtained when the assumed luminosity dispersion exceeds a factor of 2. Since the upper limit on the luminosity dispersion is not larger than approximately a factor of 2 (see Section 3.4), the bias in the best-fitting scaleheight and length caused by uncertain distances is not the leading error contribution.

3.8 The number of AGB stars in the Galaxy

The model parameters derived in the previous section can be used to approximately estimate the number of AGB stars in the Galaxy by direct integration of their number density.[7] The resulting simplified model for the number density of AGB stars with $-0.5 <$ [25]–[12] < 0 is given by

$$n(R,z) = C\ f(R)\,{\rm e}^{-|z|/h_z} + f_{\rm B}(\sqrt{R^2+z^2}), \qquad (6)$$

where

$$f(R) = {\rm e}^{-(R-R_{\rm c})/h_R}, \qquad (7)$$

for $R > R_{\rm c}$, and $f(R) = 1$ otherwise. The radius of the inner disc part where the number density does not depend on R, $R_{\rm c}$, is estimated to be 5.0 kpc. The scalelength and the scaleheight are estimated as $h_R = 1.6$ and $h_z = 0.29$ kpc, respectively. The profile of the bulge contribution, $f_{\rm B}$, is not well constrained and we assume

$$f_{\rm B}(x = \sqrt{R^2+z^2}) = \zeta_{\rm B}\,C{\rm e}^{-x/h_{\rm B}}, \qquad (8)$$

with the characteristic length $h_{\rm B} = 0.8$ kpc, and the bulge-to-disc normalization $\zeta_{\rm B} = 2$.

The normalization constant C can be determined from the observed local (at the solar radius) number density of AGB stars as

$$C = \exp\left(\frac{{\rm R}_\odot - R_{\rm c}}{h_R}\right) n(R = {\rm R}_\odot, z = 0), \qquad (9)$$

where the measured $n(R = {\rm R}_\odot, z = 0) = 150\ {\rm kpc}^{-3}$. This value is further multiplied by a correction for the incompleteness caused by selection effects estimated to be 2.9 (the variability and colour selection criteria select 35 per cent of AGB stars in the adopted colour range, see Section 2.2), to yield a best estimate $C = 2800\ {\rm kpc}^{-3}$. Note that the number density of AGB stars at the Galactic Centre is $(1+\zeta_{\rm B})C = 3C$. It is hard to determine the associated uncertainty that is dominated by the unknown selection effects and the inhomogeneity of the Galactic distribution of AGB stars, but it seems that a reasonable estimate is approximately a factor of 2.

[7] The number of stars selected in the 80° wedge, 6591, cannot be used to directly estimate the number of AGB stars in the Galaxy (by multiplying by 360/80) because the blue stars are not observed all the way to the Galactic Centre.

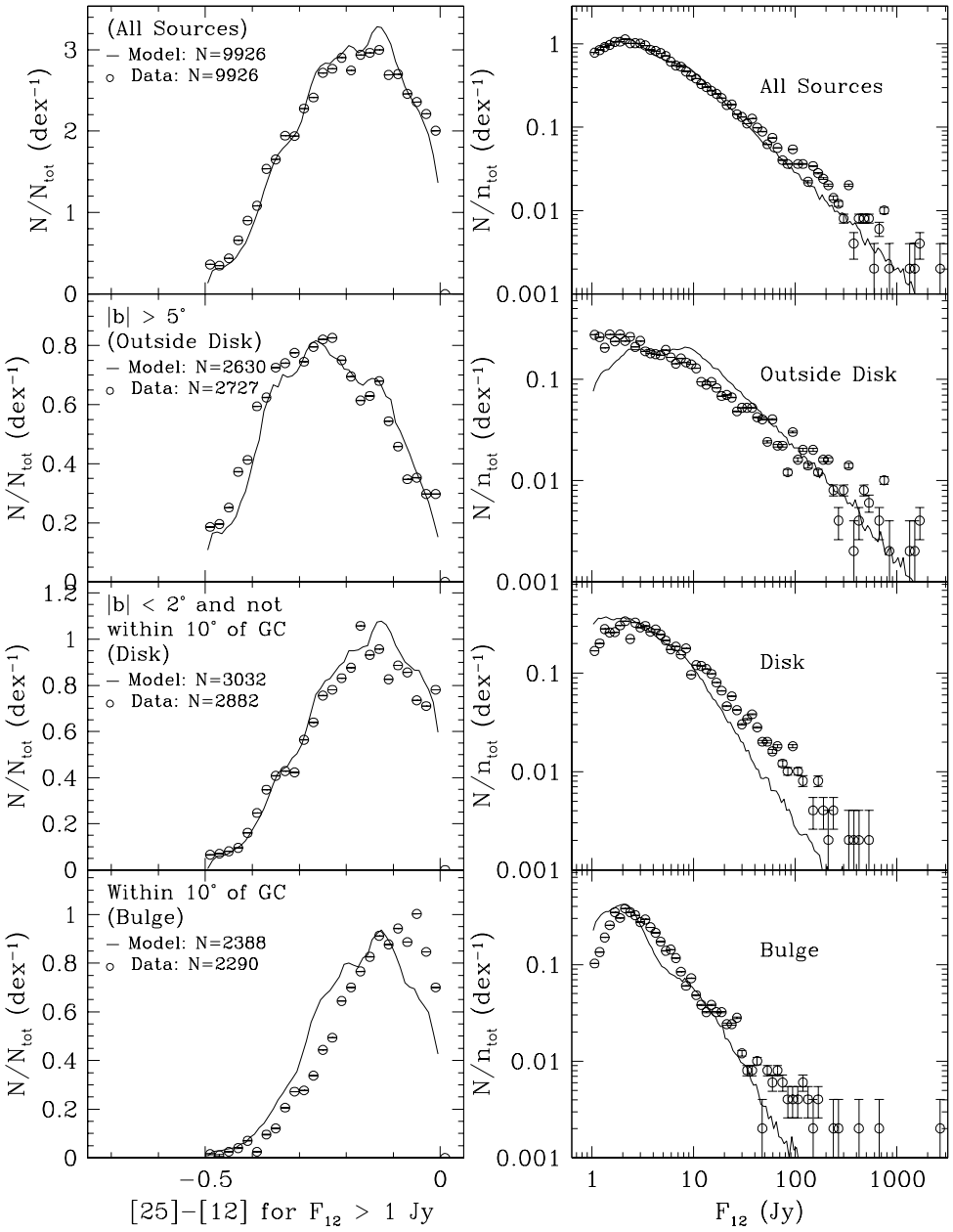

Figure 14. Comparison of the *IRAS* data and a simplified Galactic model described in the text.

The integration of the above expressions shows that the number of AGB stars in the Galaxy is

$$N_{\rm AGB} = C\pi \left[h_z R_{\rm c}^2 + 2h_z h_R (h_R + R_{\rm c}) + 8\zeta_{\rm B} h_{\rm B}^3\right]. \quad (10)$$

Using the best estimates for the model parameters, we obtain $N_{\rm AGB} = 67.7\, C\ {\rm kpc}^3 = 200\,000$. Again, this estimate is probably uncertain to within a factor of 2.

4 THE TIME EVOLUTION OF THE AGB MASS LOSS

One of the least constrained properties of AGB stars is the time evolution of their mass loss, and its dependence on fundamental stellar parameters, in particular its dependence on stellar mass. Models range from a mass-loss rate that is independent of time during the AGB phase, and fully determined by the stellar mass, to a mass-loss rate that increases exponentially with time, and is independent of the stellar mass (Habing 1996 and references therein).

The predictions of these models relevant for the data analysed here pertain to the correlations between the stellar number density, colour and z. Since the initial stellar mass correlates with z, if the mass controls the mass-loss rate then the [25]–[12] colour, which is by and large determined by mass-loss rate, should also correlate with z (i.e. the scaleheight should depend on colour). At the same time, the colour distribution would be a complicate convolution of the initial mass function and the evolutionary time-scales (which also depend on the stellar mass). On the other hand, if the mass-loss rate does not depend on the stellar mass, then there should be no correlation between the scaleheight and colour, and the distribution of colours would reflect the temporal evolution of mass-loss rate.

As shown in the middle panel in Fig. 13, there is some evidence that the scaleheight decreases with the [25]–[12] colour, as would

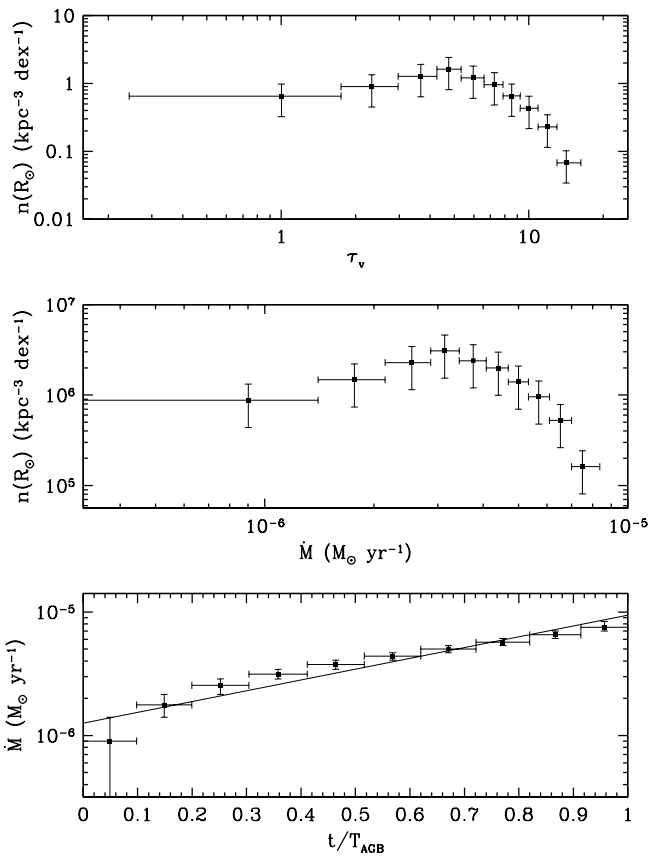

Figure 15. Derived AGB mass-loss rate as a function of $t/T_{\rm AGB}$, where $T_{\rm AGB}$ is the time spent in the observed phase of AGB stellar evolution.

be the case if only the high-mass stars develop large mass-loss rates. Since this result may be caused by various systematic effects, we only explore the alternative possibility that the mass-loss rate does not depend on the stellar mass, and is a universal function of time. This approach assumes that the scaleheight and scalelength do not depend on the [25]–[12] colour, and interprets the variation of the number density with colour as a result of temporal evolution of the mass-loss rate (see the bottom panel in Fig. 13). While, in principle, both the variation of the scaleheight and the number density with colour could be used to simultaneously constrain the dependence of mass-loss rate on stellar mass *and* time, the available data are not sufficient to derive robust conclusions in such a two-dimensional problem.

For given dust grains, the [25]–[12] colour is essentially fully determined by the dust optical depth (IE95; IE97). We use a model-derived relationship (the same models are used to derive the bolometric correction discussed in Section 3.1) between the [25]–[12] colour and the visual optical depth, τ_V, to transform the number density versus colour relation shown in the bottom panel of Fig. 13, to the number density versus τ_V relation shown in the top panel of Fig. 15.

For a given luminosity, dust grains and dust-to-gas ratio, the dust optical depth is by and large determined by the mass-loss rate (Bedijn 1987; IE95). We use a relationship derived from radiatively driven wind models with silicate dust by Elitzur & Ivezić (2001). Assuming a standard gas-to-dust mass ratio (200),

$$\dot{M} = 0.9 \times 10^{-6}\, \tau_V^{3/4}\, {\rm M}_\odot\, {\rm yr}^{-1}. \qquad (11)$$

Note that $\dot{M} \propto \tau_V^{3/4}$ rather than $\dot{M} \propto \tau_V$ caused by dust drift effects.[8] The resulting number density versus mass-loss rate relation is shown in the middle panel of Fig. 15. The observed mass-loss rate spans the range from $\sim 10^{-6}$ to $\sim 10^{-5}$ $\rm M_\odot$ $\rm yr^{-1}$ (this particular range is a consequence of the analysed range of [25]–[12] colour).

The temporal behaviour of the mass-loss rate is directly reflected in the observed distribution of mass-loss rate, assuming that the same function applies to all stars in the sample. For example, if the mass-loss rate increases quickly with time between two values, then most stars will be observed with a mass-loss rate closer to the low value. Following this assumption, we derive the mass-loss rate distribution shown by symbols in the bottom panel of Fig. 15. The error bars are computed by assuming Poisson statistics. As is evident, the increasing mass-loss rate is well described by an exponential function [i.e. $\log(\dot{M}) \propto t$], and a best fit is displayed by the line.

Note that the bottom panel of Fig. 15 displays the mass-loss rate as a function of $t/T_{\rm AGB}$, where $T_{\rm AGB}$ is the time spent in the observed phase of AGB stellar evolution (not necessarily equal to the entire duration of the AGB phase caused by the applied colour limits). This time cannot be determined from the data analysed here, and the only constraint we have on the mass-loss rate temporal behaviour is that it is well described by an exponential function. The total number of AGB stars in the Galaxy (estimated here to be $\sim$200 000) can be used to estimate $T_{\rm AGB}$ only if the number of stars in the Galaxy that become AGB stars is known, and their mean lifetime. Assuming 2×10^{10} for the former, and 10^{10} yr for the latter, reproduces the canonical AGB lifetime of 10^5 yr (Whitelock & Feast 1993 and references therein). Increasing the number of stars that undergo the AGB phase decreases the estimate of $T_{\rm AGB}$.

5 DISCUSSION

5.1 Summary of the results

We assume that AGB stars can be reliably selected using the *IRAS* variability index and the [25]–[12] colour, that their bolometric flux can be estimated from the *IRAS* F_{12} flux and the [25]–[12] colour, and that they all have the same luminosity. We estimate this luminosity to be 3500 $\rm L_\odot$, and determine the distance to each star. The analysis of the resulting Galactic distribution shows that it is well described by a simple function independent of colour.

This is the first direct (i.e. not based on fitting the number counts) estimate of the Galactic distribution of AGB stars throughout the Galaxy. It is somewhat surprising that a good description of the *IRAS* observations can be obtained by a model including only five free parameters: the scaleheight ($\sim$290 pc), the radius of the inner disc where the number density does not depend on the Galactocentric radius ($\sim$5 kpc), the scalelength ($\sim$1.6 kpc) for the exponential fall-off in the outer disc, the bulge-to-disc number density ratio at the Galactic Centre (the bulge density is twice as large as the disc density) and the overall normalization (the local density in the disc plane at the solar radius of $\sim$100 AGB stars $\rm kpc^{-3}$ for stars with $-0.5 <$ [25]–[12] < 0). The normalization is probably accurate to better than a factor of 2, and other parameters to within $\sim$20 per cent. The simplified model presented here implies that there are $\sim 10^5$ AGB stars in the Galaxy, with an uncertainty of approximately a factor of 2. While there exist other models that provide an excellent

[8] The accuracy of this formula should be comparable to other similar estimates based on infrared data (approximately a factor of 2).

description of *IRAS* counts (e.g. Wainscoat et al. 1992), they are usually much more involved than the model presented here, and often are not uniquely determined.

The final simplified model is very similar to models derived in several other studies, which are based on different methods for estimating distance. For example, Jura & Kleinmann (1992) studied the vertical scaleheight for ∼300 Mira stars with $|b| > 30^\circ$, the distance of which was determined from the period–luminosity relation. They determine the scaleheight of ∼240 pc for stars with periods, P, longer than 300 d, in agreement with the results derived here (the period and colour are correlated such that redder stars have longer periods, see Habing 1996). For stars with period shorter than 300 d they found a scaleheight of 500–600 pc (see also Feast & Whitelock 2000). We do not find evidence for such an increase of the scaleheight for the blue subsamples. A possible reason for this discrepancy is that our selection procedure missed a significant fraction of the blue stars close to the faint end (it can be expected that most stars with periods shorter than 300 d would be in the subsample, see WMF94). Another possible explanation is that some stars in the sample discussed by Jura & Kleinmann had an overestimated distance. Indeed, they point out that the stars in their sample with $P < 300$ d have approximately twice as large a velocity dispersion in the z-direction (55 km s^{-1}) as stars with $P > 300$ d. This may indicate that the former are contaminated by non-AGB stars. A third possibility is that the fraction of stars with somewhat larger scaleheights is not sufficiently large to affect the distribution for the entire sample. A fourth possibility is that the stars at large distances from the Galactic plane, discussed in Section 3.6.1, are intermediate-period Miras with large scaleheights. It is impossible to distinguish these possibilities without supplemental data.

Blommaert et al. (1993) found that the number density of (red) AGB stars falls off more steeply outside the solar circle than in the inner Galaxy. This finding agrees well with the change of slope at ∼5 kpc evident in Fig. 12. The radial scalelength determined here (1.6 kpc) is at the low end of estimates in the literature (1.8–6 kpc, Kent et al. (1991) and references therein). However, the direct comparison is inappropriate because our value is determined for $R >$ 5 kpc, while in most other studies the assumed exponential profile extends to the Galactic Centre. Fitting this function to data shown in the bottom right-hand panel in Fig. 12, we obtain a scalelength of 3 ± 1 kpc, in agreement with recent studies. It is noteworthy that studies based on infrared data yield systematically smaller scalelengths than optical studies (Wainscoat et al. 1992 and references therein).

Jura, Yamamoto & Kleinmann (1993) found that the number ratio of stars with $P > 400$ d and stars with $300 < P < 400$ d is larger at ∼1 kpc from the Galactic Centre (∼0.7) than locally (only ∼1/6). This implies that the counts ratio of blue to red AGB stars should be lower close to the Galactic Centre. However, the analysis presented here indicates that the counts of blue stars drop for $R < 2$ kpc caused by the *IRAS* flux limit. That is, we find no evidence that the ratio of red to blue AGB stars varies across the Galaxy. While this ratio may also be different in the bulge, this is not required by the *IRAS* data.

5.2 Pitfalls

Of course, all of the above results depend critically on the various adopted assumptions. For example, although the estimated sample contamination is very low (∼3 per cent, see Section 2.2), it could be somewhat higher because the AGB nature of these stars is not positively determined for each star. Similarly, the selection does not appear biased with respect to the F_{12} flux and the [25]–[12] colour, but this conclusion is also based on statistical arguments. The employed model-derived bolometric correction implies that the SEDs of all AGB stars with silicate dust are self-similar. While this assumption is certainly not strictly true, it appears to be correct to within a factor of ∼2. A systematic bias with respect to colour of the bolometric correction could produce false evidence for the dependence of the derived scaleheight and scalelength on colour. Some evidence for such a dependence is borne by the data (see Sections 3.6 and 3.7, and Fig. 13), but because of the bolometric correction uncertainties, it is not clear whether this effect is real.

It is obvious that the true AGB star luminosity function is not a δ-function; yet the shape of the distribution of stars around the Galactic Centre implies that the majority of stars have a luminosity within a factor of 2 from the median value. The assumption that all stars have the same luminosity results in smearing of their distribution such that fine details cannot be recovered. This effect may hide some interesting features, but it does not strongly affect the overall stellar distribution.

Owing to all of these uncertainties, the temporal behaviour of mass loss on the AGB cannot be strongly constrained. If the dependence of the scaleheight and scalelength is real, then the mass-loss rate increases with the stellar mass. Alternatively, if this dependence is dismissed as being caused by systematic effects, then the observed colour distribution implies that the mass-loss rate increases exponentially with time.

5.3 Possibilities for improvement

This work demonstrates that infrared observations of AGB stars are an excellent tool for studying the Galactic structure all the way to its centre and beyond. It also reveals all the pitfalls associated with the limited data set. Fortunately, these shortcomings are solvable in principle, and the AGB stars could be utilized in a study with much greater statistical power than would be possible with only the *IRAS* data.

The reliability of AGB star selection could be improved by multiwavelength multi-epoch observations, e.g. such as those obtained by van der Veen & Habing (1990), or Whitelock, Feast & Catchpole (1991). Because of the characteristic shape of SED, and its variability properties, such observations can be used to reliably separate AGB stars from other similar sources. Additionally, the observations of various masers could be utilized as yet another signature of the AGB phase (as in, for example, Jiang et al. 1997). A further important gain from the multiwavelength observations is the ability to determine the bolometric flux directly, rather than using a bolometric correction.

A study of the Galactic distribution of AGB stars would greatly benefit from an all-sky survey approximately 10 times more sensitive than *IRAS*. Such a survey would be capable of detecting AGB stars of all colours beyond the Galactic Centre, rather than only those with, for example, [25]–[12] $\gtrsim -0.3$, as with the *IRAS* data. By utilizing the fact that the distribution of stars is symmetric around the Galactic Centre, the hypothesis that the characteristic AGB star luminosity does not depend on the [25]–[12] colour could be explicitly tested on a large sample of stars. Even if obtained only for the 10×10 deg^2 area toward the Galactic Centre, such a survey would provide significant new constraints for the evolution of AGB stars and their Galactic distribution. We are currently investigating the possibility of using the 2MASS and SIRTF surveys for such a study.

ACKNOWLEDGMENTS

We acknowledge generous support by Princeton University, and by NASA grants NAG5-6734 and NAG5-11094 to GRK. We thank Tom Chester for clarifying the definition of *IRAS* variability index, and an anonymous referee for the comments that helped improve the final version.

REFERENCES

Allen C.W., 1973, Astrophysical Quantities. Athlone Press, London
Allen L.E., Kleinmann S.G., Weinberg M.D., 1993, ApJ, 411, 188
Beichman C.A., Neugebauer G., Habing H.J., Clegg P.E., Chester T.J., 1985, *IRAS* Catalogs and Atlases. US GPO, Washington, DC
Bedijn P.J., 1987, A&A, 186, 136
Binney J., Tremaine S., 1987, Galactic Dynamics. Princeton Univ. Press, Princeton
Blommaert J.A.D.L., van der Veen W.E.C.J., Habing H.J., 1993, A&A, 267, 39
Casassus S., Bronfman L., May J., Nyman L.Å., 1999, A&A, 358, 514
Chen B. et al., 2001, ApJ, 553, 184
Elitzur M., Ivezić Ž., 2001, MNRAS, 327, 403 (EI)
Feast M.W., Whitelock P.A., 2000, MNRAS, 317, 460
Feast M.W., Glass I.S., Whitelock P.A., Catchpole R.M., 1989, MNRAS, 241, 375
Gilmore G., Reid N., 1983, MNRAS, 202, 1025
Habing H., 1996, A&A, Rev., 7, 97
Habing H.J., 1988, A&A, 200, 40
Habing H.J., Olnon F.M., Chester T., Gillett F., Rowan-Robinson M., 1985, A&A, 151, L1
Herman J., Burger J.H., Penninx W.H., 1986, A&A, 167, 247
Ivezić Ž., Elitzur M., 1995, ApJ, 445, 415 (IE95)
Ivezić Ž., Elitzur M., 1997, MNRAS, 287, 799 (IE97)
Ivezić Ž., Elitzur M., 2000, ApJ, 534, L96 (IE00)
Ivezić Ž., Nenkova M., Elitzur M., 1997, User Manual for DUSTY, Internal Report, Univ. Kentucky, accessible at http://www.pa.uky.edu/~moshe/dusty
Jiang B.W., Deguchi S., Hu J.Y., Yamashita T., Nishihara E., Matsumoto S., Nakad Y., 1997, AJ, 113, 1315
Jura M., Kleinmann S.G., 1992, ApJSS, 79, 105
Jura M., Yamamoto A., Kleinmann S.G., 1993, ApJ, 413, 298
Kent S.M., Dame T.M., Fazio G., 1991, ApJ, 378, 131
Knauer T.G., Ivezić Ž., Knapp G.R., 2001, ApJ, 552, 787
Lenz D.D., Newberg J., Rosner R., Richards G.T., Stoughton C., 1998, ApJS, 119, 121
Marengo M., Ivezić Ž., Knapp G.R., 2001, MNRAS, 324, 1117
Mihalas D., Binney J., 1981, Galactic Astronomy: Structure and Kinematics. Freeman, New York
Ossenkopf V., Henning Th., Mathis J.S., 1992, A&A, 261, 567
Reid M.J., 1989, in Morris M., ed., Proc. IAU Symp. 136, The Center of the Galaxy. Kluwer, Dordrecht, p. 37
Rowan-Robinson M., 1980, ApJS, 44, 403
Rowan-Robinson M., Chester T., 1987, ApJ, 313, 413
Spitzer L., 1978, Physical Processes in the Interstellar Medium. Wiley, New York
van der Veen W.E.C.J., Breukers R., 1989, A&A, 213, 133
van der Veen W.E.C.J., Habing H.J., 1988, A&A, 194, 125
van der Veen W.E.C.J., Habing H.J., 1990, A&A, 231, 404
van der Veen W.E.C.J., Rugers M., 1989, A&A, 226, 183
Wainscoat R.J., Cohen M., Volk K., Walker H.J., Schwartz D.E., 1992, ApJSS, 83, 111
Walker H.J., Cohen M., Volk K., Wainscoat R.J., Schwartz D.E., 1989, AJ, 98, 2163
Whitelock P., Feast M., Catchpole R., 1991, MNRAS, 248, 276
Whitelock P., Feast M., 1993, in Weinberger R., Acker A., eds, Proc. IAU Symp. 155, Planetary Nebulae. Kluwer Dordecht, p. 251
Whitelock P., Menzies J., Feast M., Marang F., Carter B., Roberts G., Catchpole R., Chapman J., 1994, MNRAS, 267, 711 (WMF94)
Wouterloot J.G.A., Fiegle K., Brand J., Winnewisser G., 1995, A&A, 301, 236

This paper has been typeset from a TEX/LATEX file prepared by the author.